DUX4-stimulated genes define an antiviral defense program in human placental trophoblasts

Joshua Hatterschide[1], Liheng Yang[1], and Carolyn B. Coyne[1*]

[1]Department of Integrative Immunobiology, Duke University School of Medicine, Durham, NC, USA, Duke University Medical Center, Durham, NC, USA.

*Address correspondence:
Carolyn Coyne, PhD
3130 Medical Sciences Research Building III
3 Genome Court
Durham, NC 27710
USA
carolyn.coyne@duke.edu

Abstract

The placenta combats mother-to-fetus transmission of viruses through the antiviral activities of fetal-derived trophoblasts. Placental trophoblasts employ specialized antiviral strategies to protect against infection while preventing maternal immune rejection of the fetus. However, the full extent of how trophoblasts respond to viral infections is not well understood. To address this, we defined the transcriptional landscape of human trophoblast organoids infected with seven diverse teratogenic viruses. We found that herpesviruses, including HSV-1, HSV-2, and HCMV, did not trigger a typical interferon (IFN) response. Instead, they activated the expression of DUX4 and its downstream target genes, collectively known as DUX4-stimulated genes (DSGs). This program was highly specific for trophoblasts and was associated with cells containing low viral transcripts following HSV-1 infection, suggesting an antiviral activity. Screening of highly expressed DSGs revealed that many of them exhibited anti-herpesvirus activity, indicating the existence of an alternative antiviral pathway similar to the IFN-stimulated gene response. These findings identify DUX4 as a master regulator of a coordinated antiviral program in trophoblasts, specifically targeting a prominent family of teratogenic viruses.

17 **Graphical Abstract**

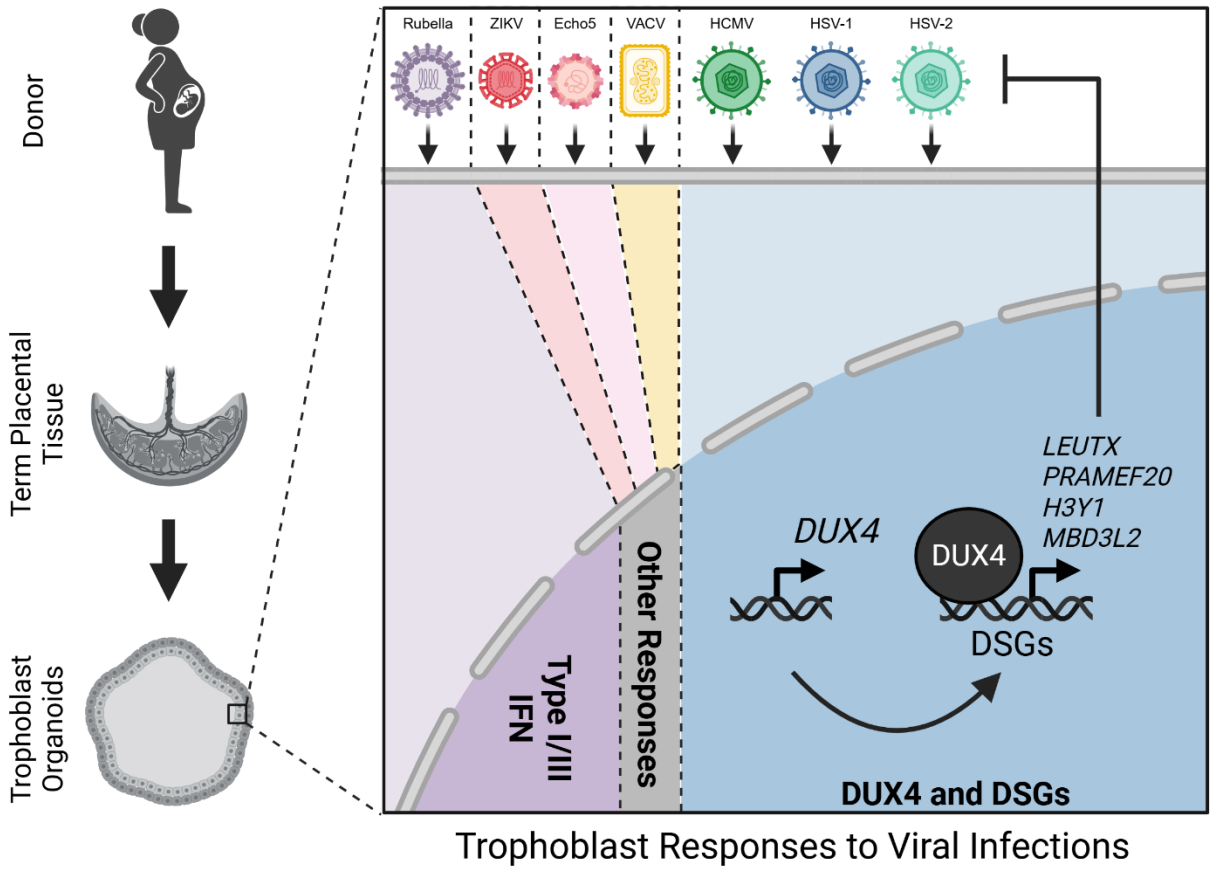

18

19

Introduction

In addition to its critical role in facilitating the exchange of nutrients, gases, and waste between mother and fetus, the placenta acts as a robust barrier against infections, protecting the vulnerable fetus from vertical pathogen transmission during gestation.[1,2] Certain pathogens, collectively referred to as TORCH pathogens (Toxoplasma, Other (e.g., enteroviruses, parvovirus B19, hepatitis B virus, syphilis, and Zika virus (ZIKV)), Rubella (RuV), Cytomegalovirus (HCMV), and Herpesviruses) are able to bypass the defenses at the maternal-fetal interface (MFI) and cause placental and/or fetal infections. These infections can lead to a variety of pregnancy complications ranging in severity and including intrauterine growth restriction (IUGR), neurodevelopmental deficits, and loss of the pregnancy.[3-7] While some TORCH pathogens are vaccine preventable and consequently rare, others remain common. For example, HCMV is estimated to be transmitted from mother to fetus in 1 out of every 200 pregnancies.[8,9] However, even in the context of a common congenital pathogen such as HCMV, most primary maternal infections during pregnancy are not transmitted to the fetus, demonstrating the efficacy of the immunological defenses present at the MFI.[10]

Fetal-derived trophoblasts form the barrier between maternal and fetal compartments at the MFI, and the antiviral properties of these cells render the placenta resistant to viral infections.[11,12] Chorionic villi of the human placenta contain several distinct subsets of trophoblasts including cytotrophoblasts (CTBs), extravillous trophoblasts (EVTs), and the syncytiotrophoblast (STB). The multinucleated STB is a single fused cell that covers the entire surface of the placenta and is in direct contact with maternal blood. CTBs are proliferative cells that lie beneath the STB and undergo fusion to grow and repair the STB layer. EVTs arise from columns of CTBs at the tips of chorionic villi, anchor the placenta to the maternal decidua (the pregnancy-specialized maternal endometrium), and facilitate the redirection of maternal blood to the intervillous space.[13] CTBs, EVTs, and the STB are differentially susceptible to viral infection and thus may respond distinctly to infections.[2] Despite their critical role as the cellular barrier at the MFI, there remains an

46 incomplete understanding of how human trophoblasts respond to and defend against viral
47 infections.

48 Responses to pathogens at the MFI must be tightly controlled, as unchecked immune signaling,
49 such as type I interferon (IFN) activation, is linked to adverse pregnancy outcomes.[14-17] Possibly
50 in response to this selective pressure, trophoblasts have evolved unique antimicrobial properties.
51 For instance, the STB constitutively secretes IFN-λs, which can act in both autocrine and
52 paracrine manners to promote IFN-stimulated gene (ISG) expression to restrict virus replication
53 in the maternal and fetal compartments of the placenta.[12,18-20] While IFN expression in most cell
54 types is only observed after the detection of pathogen associated molecular patterns (PAMPs),
55 constitutive release of IFNs from trophoblasts is stimulated by viral mimicry by host-derived
56 C19MC Alu dsRNA.[19] Evidence suggests that trophoblasts also possess IFN-independent
57 mechanisms of virus restriction. Although permissive to HCMV entry, trophoblast organoids (TOs)
58 and trophoblast stem cells have recently been shown to limit HCMV replication at the stage of
59 immediate early gene expression.[20,21] This restriction occurs even in the presence of ruxolitinib, a
60 JAK inhibitor that inhibits both type I and type III IFN signaling.[20] However, the role of IFN-
61 independent pathways in virus restriction in trophoblasts remains largely unexplored, highlighting
62 a critical gap in our understanding.

63 Gaps in our knowledge surrounding how human trophoblasts respond to and defend against
64 virus infection can be attributed to the paucity of tractable systems to model the human MFI. The
65 anatomy of the MFI in many animal models is divergent from that of humans,[22,23] and animal
66 models also often require the use species-specific viruses (as in the case for HCMV)[24,25] or
67 immunodeficient or humanized animal models (as in the case of ZIKV in mice).[26] Human placental
68 explants,[27,28] isolated primary human trophoblast cells,[12] choriocarcinoma cell lines,[29] and
69 immortalized EVT cell lines[30] have all been employed to study human pathogens in their natural
70 host cells. However, these models either have a limited window of viability or lack physiological
71 properties of *in vivo* trophoblasts.[31] Trophoblast organoids (TOs) are an *in vitro* model of the

placenta that is able to overcome some of the limitations of previous models. TOs and matched maternal decidua gland organoids (DOs) can be derived from chorionic villi at early and late stages of gestation.[20,32,33] TOs spontaneously differentiate into EVTs and the STB and constitutively secrete hormones such as human chorionic gonadotropin (hCG) and immune molecules such as IFN-λs that are naturally secreted by trophoblasts *in vivo*.[20]

In this study, we profiled the transcriptional responses of TOs to seven teratogenic viruses to define cell-intrinsic mechanisms of virus restriction in trophoblasts and to determine whether these cells responded in a virus-specific manner. We found that TOs mounted distinct responses to RNA and DNA viruses, with the transcription factor DUX4 dominating the response to herpesviruses. DUX4 is a primate-specific pioneering transcription factor that participates in zygotic genome activation and is typically restricted to the 4-8 cells stages of embryonic development.[34] DUX4 is heterochromatinized in adult somatic cells, and aberrant expression of DUX4 in adult muscle cells is the cause of facioscapulohumeral muscular dystrophy (FSHD).[35,36] Comparative transcriptional profiling in TOs and DOs derived from matched donor tissue infected with HCMV and HSV-1 revealed that the DUX4 program is enriched in TOs, which occurs independent of constitutive type III IFN signaling. Using single cell RNA sequencing (scRNAseq), we characterized the DUX4 program in trophoblasts in the context of both an inducible DUX4 expression system and HSV-1 infection. DUX4 and accompanying DUX4-stimulated genes (DSGs) were observed to define a low viral gene expression trajectory in HSV-1 infected TOs. To explore the possible antiviral activity of DSGs, we performed high-content screening of the 30 top-most induced DSGs in TOs for antiviral activity against herpesviruses in naturally permissive cells. Analogous to ISGs in the IFN pathway, we observed redundancy in the antiviral activity of DSGs. Expression of DUX4 has been observed following herpesvirus infection in other systems and a few DSGs were previously reported to restrict herpesvirus replication.[37,38] However, these data shift our understanding of DUX4 and DSGs from a few isolated antiviral genes to a concerted antiviral signaling program that retains key hallmarks of ISGs, including a robust and overlapping

98 antiviral gene induction mechanism. Together, these findings unveil a human trophoblast-
99 enriched anti-herpesvirus pathway that mirrors the functional principles of the IFN response,
100 providing new insights into host defense strategies against viral infections at the maternal-fetal
101 interface.

102 ## Results

103 ### Human trophoblast organoids respond distinctly to diverse viruses

104 To directly compare how human placental trophoblasts respond to infection with teratogenic
105 viruses, TOs from two male donors and one female donor were infected with seven teratogenic
106 viruses that belong to diverse virus families. These viruses included three herpesviruses: HCMV,
107 HSV-1, HSV-2, a poxvirus: Vaccinia virus (VACV), and three positive sense RNA viruses:
108 echovirus 5 (Echo5), rubella virus (RuV), and Zika virus (ZIKV). RNA was collected from mock
109 and infected TOs and sent for polyA-selection bulk RNA sequencing. Reads were mapped to both
110 the human and viral genomes. We observed minimal mapping of reads to the viral genomes in
111 mock samples and little donor-to-donor variation in viral read levels in infected samples **(Figure**
112 **S1A)**. We have previously reported that HCMV replication is impaired in TOs. However, entry and
113 gene expression were confirmed based on high quantities of reads mapping to the HCMV genome
114 **(Figure S1A)**. In contrast, several of the other viruses exhibited evidence of replication, albeit at
115 low levels in some cases. Fluorescent protein expression from HSV-1 (GFP) was detectable by
116 fluorescence microscopy, and HSV-1 and HSV-2 both induced cytopathic effect (CPE) in TOs
117 **(Figure S1B)**. Fluorescent tag expression from VACV (YFP) was also visible by fluorescence
118 microscopy **(Figure S1C)**. CPE was observed in TOs following RuV infection, but not following
119 infection with either Echo5 or ZIKV **(Figure S1C-D)**. Consistent with this observation, RuV was
120 the only positive sense RNA viruses that yielded high levels of both positive and negative strand
121 genomic reads in all donors, suggesting it is the only one of these viruses readily engaging in
122 productive replication **(Figure S1E)**. For the remaining analyses, reads mapping to the virus
123 genomes were excluded to focus on host cell responses.

124 Differential gene expression analysis was conducted using the DESeq2 package,
125 incorporating donor as a factor in the statistical model to account for variability between individual
126 donors.[39] Differentially expressed genes (DEGs) were defined as host genes with Log_2 (fold-
127 change) > 1 and adjusted *p*-value < 0.05. The differences in magnitude of the induced responses

128 ranged from zero DEGs following ZIKV infection to 5453 DEGs following VACV infection **(Figure**
129 **1A-G and Table S1)**. We also observed variability in the directionality of responses. HSV-1, HSV-
130 2, and RuV all led to substantially more upregulated DEGs than downregulated. HCMV and VACV
131 both led to a relatively even distribution between upregulated and downregulated DEGs. Echo5
132 was the only virus with a response that skewed toward downregulation **(Figure 1A-G)**. The small
133 transcriptional responses elicited by Echo5 and ZIKV may arise from impaired virus replication in
134 TOs, which would lead to lower levels of pathogen associated molecular pattern (PAMP) detection
135 and a diminished transcriptional response. This is consistent with the observation that these
136 viruses had the lowest quantities of viral reads **(Figure S1A and E)**. Pairwise comparisons
137 between each infection condition revealed some overlap in upregulated and downregulated DEGs
138 between these diverse viruses **(Figure 1H).** However, after excluding Echo5 and ZIKV (due to
139 their limited responses), only two DEGs were upregulated by all of the five remaining viruses:
140 *EGR3* and *THBS1*. This suggests that TOs respond distinctly to infection in a virus-specific
141 manner.

142 To further categorize these responses, we performed a principal component analysis (PCA).
143 Four groups were found to segregate from the mock-infected samples along the first four principle
144 components: HSV-1- and HSV-2-infected, VACV-infected, RuV-infected, and HCMV-infected
145 **(Figure 1I)**. As expected, Echo5- and ZIKV-infected samples clustered closely with the mock-
146 infected samples. We next analyzed the loadings from the PCA to identify sets of genes that
147 defined these unique responses. The response to VACV was predominantly defined by genes
148 encoding histone variants such as *H3C1* and *H4C2* **(Figure 1J, middle left)**. RuV was the only
149 virus that induced type-I and type-III IFN genes such as *IFNB1* and *IFNL1* along with downstream
150 IFN-stimulated genes (ISGs) including *OASL*, *IFIT2,* and many others **(Figure 1J, middle right)**.
151 The unique response to HCMV was defined by genes including *IVL*, *IL1RN*, and *MPZL2* **(Figure**
152 **1J, right)**. HSV-1- and HSV-2- infected samples were defined by tripartite motif family genes such

153 as *TRIM43* and *TRIM49*, and preferentially expressed antigen of melanoma family genes such
154 as *PRAMEF8* and *PRAMEF12* **(Figure 1J, left)**.
155 Many of the genes that defined the HSV-1- and HSV-2- infected samples were also induced
156 by HCMV. In fact, there were 28 genes induced by all three herpesviruses **(Figure S1B)**. Notably,
157 most of these shared DEGs were induced by herpesvirus infections and were not induced by any
158 other viruses **(Figure S1C)**. These findings suggest the existence of a herpesvirus-specific
159 pathway activated in trophoblasts.
160

161 **Trophoblasts respond to herpesviruses with DUX4-stimulated genes**

162 Several of the shared differentially expressed genes induced by HSV-1, HSV-2 and HCMV,
163 such as *TRIM43*, are putative targets of the transcription factor DUX4. DUX4 is a pioneering
164 transcription factor that is normally expressed during embryogenesis between the four-cell and
165 eight-cell stages[34] and is pathogenic when aberrantly expressed in adult muscle cells.[35,36] DUX4
166 has also been shown to be upregulated following HSV-1 infection.[37] In the TO infection bulk
167 RNAseq analyses, *DUX4* expression was up-regulated in all donors by HSV-1 and HSV-2 and by
168 two donors by HCMV **(Figure 2A)**. DUX4 was not detected in any other infection conditions.
169 However, *DUX4* expression is notoriously difficult to detect even using next generation
170 sequencing methods.[40,41] Therefore, we confirmed the expression of *DUX4* and the DUX4
171 transcriptional-target, *TRIM43*, only in herpesvirus-infected samples in all three donors using
172 qRT-PCR **(Figure S2A-B)**.
173 DUX4 has never been studied in trophoblasts, and DSGs in these cells have yet to be defined.
174 To characterize DSGs in trophoblasts, we developed a model of DUX4 expression in TOs. TOs
175 from three donors were transduced with a lentiviral vector encoding codon-optimized DUX4 under
176 a doxycycline-inducible promoter (iDUX4). Transduced organoids were selected with puromycin,
177 and expression of DUX4 upon treatment with doxycycline was confirmed by immunofluorescence
178 **(Figure 2B)**. One strength of the TO model is that they retain the capacity to differentiated into

179 several lineages of trophoblasts present in the placenta *in vivo*. To define DSGs across
180 trophoblast cell types, and to determine whether there were trophoblast cell type-specific DSGs,
181 doxycycline-treated and mock-treated organoids from three donors were dissociated and
182 analyzed by single-cell (sc)-RNAseq. A total of 23,981 doxycycline-treated cells and 23,233 mock-
183 treated cells passed quality control and were used for further transcriptional analysis following
184 integration to correct for donor and batch effects. Cluster analysis revealed 11 cell clusters that
185 were present in both conditions **(Figure 2C and Figure S2C)**. The identities of the clusters were
186 defined by the expression of canonical trophoblast marker genes[42-44] **(Figure S2E-F)**. The
187 proliferative CTB clusters (CTBp-1, -2, and -3) were defined by high expression of *MKI67*, *CCNA2*,
188 *PCNA*, and *TOP2A*. CTB clusters (CTB-1, -2, -3, and -4) were defined by cells that express high
189 levels of the pan-trophoblast markers *PAGE4*, *PEG10*, *SMAGP*, and *TP63*, but lacked expression
190 of more specialized programs. Of note, CTBp-1 and CTB-4 also expressed markers of cell column
191 CTBs such as *ITGB6*, *ATF3*, *PLAC8*, and *PLAU*. Cells in the process of fusing into the STB
192 (STBpre) were defined by the expression of the endogenous retroviral elements that mediate and
193 modulate fusion such as *ERVV-1*, *ERVFRD-1*, *ERVW-1*, and *ERVE-1*. Markers of STB function
194 including *HOPX*, *SDC1*, *CGB5*, and *PSG3* were used to define the STB cluster. Two clusters
195 were classified based on high iDUX4 expression in the doxycycline-treated samples (DUX4-high-
196 1 and DUX4-high-2). Based on the expression of other markers, these clusters most closely
197 resembled CTBs **(Figure S2E)**. The presence of select cells in the "DUX4-high" clusters in mock-
198 treated samples is likely due to leaky expression of iDUX4. The DUX4-high-1 cluster expands
199 from an average of 1.6% of the mock-treated cells to an average of 11.6% of the doxycycline-
200 treated cells **(Figure S2D)**. The remaining clusters occupied a similar proportion of cells between
201 donors and conditions.

202 We first sought to identify genes that were broadly controlled by DUX4 across cells in the
203 dataset. We calculated the Pearson's correlation coefficient (r) between the expression of iDUX4
204 and other genes across all cells. One hundred and fifty genes were found to positively correlate

205 with iDUX4 expression with r > 0.4 suggesting they were stimulated by iDUX4 and could be
206 classified as DSGs **(Figure 2D and Table S2)**. To test whether these genes were similar to DSGs
207 in other cell types, we generated a list of 101 cell-type-independent DSGs (DUX4.101) by
208 reanalyzing and comparing bulk RNAseq datasets in which DUX4 was overexpressed in iPSCs
209 (a model of DUX4 in embryogenesis)[34] and MB135 cells (a model of DUX4 in muscular
210 dystrophy)[45] **(Figure S3A-C and Table S3)**. The expression of many of the genes in the
211 DUX4.101 list strongly correlated with iDUX4, suggesting the DUX4 program in TOs is similar to
212 that of other cell types **(Figure 2D)**. We also confirmed overlap between the DUX4.101 list and
213 genes controlled by DUX4 in TOs by performing bulk RNAseq on doxycycline-treated and mock-
214 treated organoids **(Figure S3D-E and Table S3)**. While there were many genes uniquely
215 modulated by iDUX4 in TOs, these data demonstrate that the canonical DUX4 program is induced
216 in trophoblasts. 98 of the genes that correlated with iDUX4 expression with r > 0.4 were not a part
217 of the iDUX4 list, including *GTF2F1*, *PTP4A1*, *DBR1*, *ODC1*, *SOX15* amongst others.

218 We next investigated which trophoblast cell types predominantly expressed the DUX4 pathway
219 and whether it could be activated in a trophoblast cell type-specific manner. Expression of genes
220 in the DUX4.101 list were elevated in the doxycycline-treated samples and predominantly found
221 in the two DUX4-high clusters **(Figure 2E-F)**. This demonstrates that cells that express iDUX4
222 are transcriptionally distinct enough to cluster separately from other trophoblasts. As iDUX4
223 expression could also be observed in the non-DUX4-high clusters **(Figure 2F)**, we next defined
224 the impact of iDUX4 expression in these cell types. We performed pseudobulk analysis to identify
225 DEGs between the doxycycline-treated and mock-treated samples for each cluster. Although
226 there were cluster-specific differences in DEGs, genes in the DUX4.101 list were found to be
227 among the most highly differentially expressed genes across all clusters **(Figure 2G and Table**
228 **S4)**. These data demonstrate that many of the canonical DSGs are also induced by DUX4
229 expression in trophoblasts and that DUX4 expression is capable of driving the expression of these
230 genes in all trophoblast lineages.

231 Finally, we determined whether any of the DEGs induced in TOs in response to herpesvirus
232 infections were DSGs. We found that the DUX4.101 list significantly overlapped with the top 100
233 DEGs induced by HCMV, HSV-1, and HSV-2, while overlapping by only one gene with the top
234 DEGs induced by VACV and zero with RuV **(Figure 2H and Figure S3F-K)**. HCMV may have
235 induced fewer DSGs than HSV-1 or HSV-2 due to its impaired replication in trophoblasts [20,21].
236 Based on these data, we conclude that many of the shared genes induced by herpesviruses in
237 TOs are DSGs.
238

239 **DUX4-stimulated genes are induced to higher levels in trophoblast organoids than**
240 **maternal-derived decidua epithelial organoids**

241 Trophoblasts restrict HCMV replication.[20,21] For example, we have previously reported that
242 fluorescently-tagged HCMV strains express high levels of fluorescent protein in maternal DOs
243 while exhibiting minimal tag expression in matched TOs.[20] Unlike HCMV, HSV-1 exhibits signs of
244 replication in TOs, including fluorescent tag expression and promoting CPE **(Figures S1B)**. To
245 test whether HSV-1 replication is impaired in TOs compared to DOs, both types of organoids were
246 mock-treated or infected with HSV-1 (MOI of 0.1) enabling multiple rounds of replication. Organoid
247 media was sampled at 1, 2, and 3 dpi, and HSV-1 infectious virus was quantified. While TOs
248 indeed supported the production of infectious HSV-1 particles as predicted, we observed an
249 average of 8.4-fold lower titers produced from TOs than matched maternal DOs across time points
250 **(Figure 3A-B)**. These data suggest that TOs restrict HSV-1 replication.

251 TOs differentially respond to HCMV when compared to maternal DOs, suggesting that there
252 may be trophoblasts-specific responses to herpesvirus infection.[20] We next assessed whether
253 DUX4 and DSGs were differentially induced in TOs and DOs following herpesvirus infections.
254 Matched TOs and DOs were mock-treated or infected with HSV-1 (MOI of 5). RNA was collected
255 and sent for polyA selection bulk RNA sequencing. Additionally, we reanalyzed published RNA
256 sequencing data from infection of TOs and DOs with the HCMV strains TB40/E and AD169r (a

257 clone of AD169 engineered to express the HCMV pentameric complex).[20,46] All RNA sequencing
258 datasets were remapped to the human transcriptome following the same pipeline and analyzed
259 using DESeq2 **(Table S5)**. We found that DUX4 expression was more than 9-fold higher in TOs
260 than DOs following infection with HCMV TB40/E **(Figure 3C)**, HCMV AD169r **(Figure 3D)**, and
261 HSV-1 **(Figure 3E)**. Analysis of the top 100 upregulated DEGs following each infection revealed
262 greater overlap between the DEGs of TOs and the DUX4.101 list compared to the DEGs of DOs
263 **(Figure 3F)**. While these DSGs were highly induced in TOs, nearly all of them were not induced
264 in DOs following infection with HCMV TB40/E or HCMV AD169r **(Figure 3G and Figure S4A-D)**.
265 Although DSGs were induced following HSV-1 infection in both TOs and DOs, all were induced
266 between 6- and 50-fold more in TOs **(Figure 3G and Figure S4E-F)**. We used qRT-PCR to
267 confirm enhanced expression of *DUX4* and the DSGs *TRIM43B* and *PRAMEF1* in three donors
268 of TOs compared to three donors of DOs following HCMV TB40/E infection **(Figure S4G-I)**. These
269 data demonstrate that trophoblasts respond with higher expression of *DUX4* and DSGs than
270 maternal decidua epithelial cells.
271

272 **Expression of DUX4 and DSGs is not dependent on constitutive type-III IFN signaling**

273 The mechanisms by which DUX4 and DSG expression are induced by herpesviruses remain
274 unknown. Additionally, the signaling pathways that modulate this program to drive its heightened
275 expression in TOs have yet to be identified. Trophoblast stem cells, another *in vitro* model of
276 trophoblasts, can be induced to differentiate into EVTs and the STB under specific culture
277 conditions.[47] Upon reanalysis of previously published RNA sequencing data from trophoblast
278 stem cell responses to infection with mCherry-tagged HCMV,[21] we found that infection of STB-
279 differentiated trophoblasts elicited between 4- and 960-fold higher levels of DUX4 and DSGs than
280 mCherry-positive undifferentiated trophoblasts stem cells **(Figure S4J)**. EVT-differentiated
281 trophoblasts infected with HCMV also elicited a greater DUX4 and DSG response than
282 undifferentiated TSCs, but less so than the STB-differentiated condition. These data suggest that

283 trophoblast differentiation, especially towards the STB, may drive the high levels of this program
284 observed in TOs.

285 Trophoblasts constitutively secrete type III IFNs, which is a major innate immunological
286 difference between TOs and DOs.[20] Additionally, type III IFNs are produced by the STB.[18]
287 Although DUX4 and DSG expression has not been previously linked to type-III IFN signaling, it
288 could explain the increased expression of DUX4 and DSGs in TOs over DOs and in the STB over
289 other trophoblasts. To test this, we generated *IFNLR1* knockout (KO) TOs using CRISPR-Cas9
290 and a single guide RNA (sgRNA) targeting exon three of the *IRNLR1* locus. To validate KO of
291 *IFNLR1* genetically, we amplified the sgRNA target site using high-fidelity PCR and sequenced
292 the product using Sanger sequencing. Using the ICE tool (Synthego) to predict the mixture of
293 insertions and deletions present in the mixture, we found -19 bp and -10 bp deletions >95% of the
294 sequences in the IFNLR1 KO clone **(Figure 4A-B)**. To test whether IFNLR1 KO TOs are
295 responsive to type-III IFNs, parental and IFNLR1 KO organoids were treated with recombinant
296 IFNλ3. RNA was collected and qRT-PCR was used to measure the expression of several ISGs.
297 Whereas *OASL* and *MX1* were induced ~ 5-fold and 10-fold respectively in the parental TOs
298 treated with IFNλ3, neither was induced in IFNLR1 KO TOs **(Figure 4C-D)**. Additionally, *OASL*
299 and *MX1* were expressed at a significantly lower baseline-level in IFNLR1 KO cells, likely due to
300 disruption of constitutive autocrine type III IFN signaling. IFNLR1 KO and parental cells were
301 infected with HSV-1 to induce the expression of DUX4 and DSGs. RNA was collected from mock
302 and infected organoids and qRT-PCR was used to measure the expression of the HSV-1
303 immediate early transcript ICP4, *DUX4*, and the DSGs: *TRIM43* and *PRAMEF1*. HSV-1 ICP4 was
304 expressed at similar levels in parental and IFNLR1 KO cells, suggesting that type III IFN signaling
305 does not restrict HSV-1 replication **(Figure 4E)**. *DUX4* expression was increased in IFNLR1 KO
306 TOs and *TRIM43* and *PRAMEF1* were expressed at similar levels in control and KO organoids
307 **(Figure F-H)**. These data suggest that the increased expression of *DUX4* and DSGs in TOs
308 occurs through a mechanism independent of type-III IFN signaling.

309

310 **DUX4 expression is inversely correlated with HSV-1 gene expression in trophoblast**
311 **organoids**

312 In comparison to matched maternal DOs, TOs restricted the replication of HCMV and HSV-1
313 and simultaneously expressed substantially higher levels of DUX4 and DSGs **(Figure 3)**. This
314 correlation suggests that these genes may contribute to making TOs less permissive to
315 herpesvirus replication. To explore this hypothesis, we first asked how DUX4 expression in
316 trophoblasts correlated with HSV-1 gene expression. TOs were mock-infected or infected with
317 HSV-1 (MOI 5; GFP tagged to UL25) and then DUX4 expression was imaged by
318 immunofluorescence confocal microscopy. DUX4 protein expression was only observed in
319 infected trophoblasts within TOs, confirming our earlier transcriptomics results **(Figure 5A)**.
320 Additionally, we noted that DUX4 expression was observed primarily in cells with little to no
321 expression of the HSV-1 GFP tag. To confirm this observation, we quantified the nuclear intensity
322 of DUX4 and the HSV-1 GFP tag across thousands of cells and found that DUX4 intensity
323 inversely correlated with HSV-1 GFP intensity **(Figure 5B)**, which was consistent across
324 independent infections **(Figure 5C)**. These data are consistent with the hypothesis that DUX4
325 and DSGs may contribute to restricting herpesvirus replication in TOs.

326

327 **DUX4-stimulated genes define a low viral gene expression trajectory in HSV-1-infected**
328 **trophoblast organoids**

329 To further define the relationship between the DUX4-DSG program and herpesvirus infections
330 in trophoblasts, we next investigated which trophoblast cell types expressed this program in
331 response to infection and examined how the expression of these genes compared to that of viral
332 genes. HSV-1-infected and mock-infected organoids from two donors were dissociated and
333 analyzed by scRNAseq. A total of 14,846 HSV-1-infected cells and 13,881 mock-infected cells
334 passed quality control and were used for further analysis following integration to correct for donor

335 and batch effects. Clustering analysis revealed 11 clusters of cells that were present in both
336 conditions **(Figure 6A and Figure S5A-C)**. The identities of the clusters were defined by the
337 expression of the canonical trophoblast marker genes described above **(Figure S5D-J)**.

338 We first investigated which cells expressed DUX4/DSG and HSV-1 transcripts. We found that
339 *DUX4* and DSGs were only expressed in HSV-1-infected samples, with one CTB cluster exhibiting
340 particularly high levels of expression (termed "DUX4-high"). *DUX4* and DSG expression was also
341 high in the STB cluster, consistent with the results observed in the trophoblast stem cell model
342 **(Figure 6B and Figure S5I)**. In contrast, most HSV-1 transcripts, including all transcripts
343 classified as late genes (γ1 and γ2) were expressed highest in a distinct CTB cluster (termed
344 "HSV-1-high") **(Figure 6C and Figure S5J-K)**. A handful of immediate early (α), early (β), and
345 unclassified HSV-1 genes were expressed at comparable or higher levels in the DUX4-high
346 cluster when compared to the HSV-1-high cluster. As HSV-1 genes expression could be observed
347 outside of the HSV-1- and DUX4-high clusters **(Figure 6B-C)**, we next investigated how HSV-1
348 infection impacted gene expression in these clusters. We performed pseudobulk analysis to
349 define differential gene expression between the HSV-1-infected and mock-infected samples in
350 each of these clusters **(Figure 6D and Table S6)**. Other than HSV-1 genes, DSGs were found to
351 be amongst the most highly differentially expressed genes in all clusters. These data demonstrate
352 that all trophoblast lineages in TOs can respond to HSV-1 infection with the expression of DUX4
353 and DSGs.

354 The observation that peak DUX4/DSG expression and peak HSV-1 transcript expression were
355 found in separate HSV-1-infected clusters suggests two possibilities: 1) that DUX4 and DSG
356 expression precedes maximal HSV-1 gene expression during the normal course of replication, or
357 2) that DUX4 and DSG expression defines a distinct fate of HSV-1-infected cells in which
358 replication is impaired. To determine which was the case, we performed trajectory analysis which
359 seeks to computationally infer the ordered progression of cells along a "pseudotime." Cells from
360 HSV-1-infected samples with > 0.1% of reads mapping to the HSV-1 genome were re-analyzed

361 independently **(Figure 6E)**. Clustering yielded eight clusters that were defined as described for
362 previous analyzes **(Figure S5G-J)**. Trajectories were predicted using the Slingshot algorithm
363 starting with the CTB-2 cluster and with undefined end clusters.[48] Three trajectories were inferred,
364 one that leads toward peak DSG expression (pseudotime 1), one that leads toward the peak of
365 HSV-1 gene expression (pseudotime 2), and one that follows differentiation into the STB
366 (pseudotime 3) **(Figure 6F)**. We performed pseudobulk analysis comparing cells at the termini of
367 pseudotime 1 and 2 to determine differential gene expression. We found that all but one HSV-1
368 transcript was more highly expressed in terminus 2 than 1 **(Figure 6G)**. Conversely, 64 DSGs
369 from the DUX4.101 list were more highly expressed in terminus 1 than 2. Four DSGs followed the
370 opposite pattern, and the remainder were not statistically significant. To visualize gene expression
371 patterns along these trajectories, fitGAM was used to calculate the average expression of HSV-1
372 transcripts and DSGs along pseudotime trajectories 1 and 2. While HSV-1 transcripts increased
373 along pseudotime 1, most reached only a small fraction of peak expression **(Figure 6H)**. All but
374 two HSV-1 transcripts instead reached maximum gene expression along pseudotime 2. DSGs
375 followed the opposite pattern. Nearly all DSGs reached peak expression along pseudotime 1,
376 while they reached only a fraction of peak expression along pseudotime 2 **(Figure 6I)**.
377 Interestingly, peak DSG expression comes after the rise and fall of HSV-1 genes expression along
378 pseudotime 1. This pattern is borne out by the expression of representative features such as the
379 percent of transcripts mapping to HSV-1, GFP expression from the HSV-1 genome, and
380 expression of DSGs *TRIM49* and *PRAMEF1* **(Figure 6J-K and Figure S5J)**. Taken together,
381 these data suggest that high DSG expression defines a low viral gene expression trajectory in
382 HSV-1-infected trophoblasts.
383

384 **DUX4-stimulated genes exert anti-herpesvirus activity**

385 Given that DUX4 and DSGs were highly upregulated in response to herpesviruses and defined
386 a trajectory associated with low viral gene expression following infection, we next sought to

387 determine whether these genes exhibited anti-herpesvirus activity. As the cause of FSHD, many
388 studies have attempted to engineer cells to block or impair DUX4 expression.[49] In genetically
389 normal cells, hundreds of copies of DUX4 coding sequence are repeated within D4Z4 arrays that
390 are located in the proximal sub-telomeric domains of chromosomes 4 and 10. D4Z4 has additional
391 homologous regions in many other chromosomes.[50] For this reason, traditional CRIPSR-Cas9
392 editing within the DUX4 ORF is not generally employed as it would generate many double-
393 stranded breaks, leading to genome instability and off-target effects.[49] Instead, studies have
394 employed CRISPR interference (CRISPRi),[51] CRISPR/Cas9-directed base editing,[52] and
395 dominant-negative DUX4 constructs,[53] all with varying degrees of knockdown efficiency. We
396 attempted several similar methods of impairing DUX4 activity in TOs including *DUX4*-targeting
397 shRNAs **(Figure S6A-D)**, CRISPRi targeting the transcription start site of the *DUX4* locus **(Figure**
398 **S6E-G)**, and a dominant-negative DUX4 construct where the transactivation domain was
399 swapped for the KRAB domain of ZIM3 **(Figure S6H-L)**. Although we achieved modest
400 suppression of *DUX4* using shRNAs and of the DSGs *TRIM43* and *PRAMEF1* using the DUX4-
401 ZIM3 construct, DSGs in these contexts were still expressed at ~250- and 500-fold more than in
402 mock samples (which were at or near the limit of detection). Accordingly, these interventions had
403 insignificant impact on HSV-1 gene expression **(Figure S6D and L)**. For this reason, we decided
404 to instead interrogate the top DSGs induced by herpesviruses in TOs for anti-herpesvirus activity.
405 The biological functions of DSGs are largely unknown. Therefore, we systematically screened
406 individual DSGs for antiviral activity against HCMV and HSV-1 using an overexpression system
407 in cells permissive to virus replication. We selected DSGs that were highly induced in response
408 to iDUX4 expression, and HCMV TB40/E, HCMV AD169r, or HSV-1 infection **(Figure S7A)**. Many
409 DSGs were within transposable elements, causing them to have many orthologues in the human
410 genome which are often other DSGs.[34] Among DSGs with >90% peptide identity, a single ORF
411 was selected **(Figure S7B)**. The remaining genes were prioritized to a list of 30 based on median
412 $\log_2$ (fold-change) in TO datasets **(Figure S7C)**. Codon-optimized ORFs of these genes were

413 cloned into lentiviral expression vectors that co-expressed puromycin resistance and Tag2BFP
414 on a polycistronic transcript **(Figure 7A)**. MRC5 cells, which are permissive to HCMV and HSV-
415 1, were arrayed in 96-well plates and transduced with these lentiviruses as well as a control
416 lentivirus (ORF_Stuffer) and a vector expressing a codon-optimized *DUX4* ORF. Cells were
417 selected with 2 µg/mL puromycin for 48 h. Cells were then infected with 5 x 10^4 pfu / well of HCMV
418 TB40/E (mCherry) or 5 x 10^3 pfu / well of HSV-1 (GFP-UL25). These infection conditions were
419 chosen to observe a single round of HCMV replication in a high percentage of cells over 96 h,
420 while allowing for multiple rounds of HSV-1 replication over a similar timespan. Replication
421 progression was monitored over time using high-content automated fluorescence microscopy
422 **(Figure 7A)**. Overexpression of six DSGs as well as DUX4 exhibited cell toxicity in MRC5 cells
423 **(Figure S7D-E)**.

424 Fluorescence intensity of the exogenously expressed tags was quantified, and hits at each
425 timepoint were defined as conditions that reduced the fluorescence intensity to less than half of
426 that of ORF_Stuffer **(Figure S7F)**. We observed 17, 21, 18, and 15 hits for HCMV at 1, 2, 3, and
427 4 dpi respectively **(Figure 7B and D and Figure S8A-C)**. 13, 10, and 8 hits were observed for
428 HSV-1 at 1, 2, and 3 dpi **(Figure 7C and E and Figure S8E-F)**. Ten genes consistently restricted
429 replication of both viruses: *CCNA1*, *FRG2*, *H3Y1*, *LEUTX*, *MBD3L2*, *PRAMEF2*, *PRAMEF8*,
430 *PRAMEF20*, *PRR20D*, and *TRIM49* **(Figure 7F-G)**. A handful of candidates were found to be
431 antiviral to HCMV but not HSV-1. These included *PRAMFE12* and *ZSCAN4*, both of which
432 consistently reduced mCherry expression from HCMV to less than 25% of ORF_Stuffer while
433 having minimal impact on GFP expression from HSV-1 **(Figure 7G)**. The top hits from both viruses
434 suppressed fluorescence protein expression throughout all timepoints **(Figure S8D and G)**.

435 Reduction in fluorescent tag expression does not necessarily indicate a measurable decrease
436 in virus output. To explore the magnitude of the impact of DSGs on herpesvirus virion production,
437 MRC5 cells were transduced with seven of the top DSGs or the ORF_Stuffer control vector and
438 selected with puromycin as described above. These cells were then infected with HCMV TB40/E

439 mCherry (MOI of ~2) or HSV-1 GFP-UL25 (MOI ~0.1) followed by washing three times with PBS
440 to remove residual inoculum. Media was collected at 4 dpi for HCMV and 3 dpi for HSV-1 allowing
441 for a single round of replication or multiple rounds of replication respectively. Quantification of
442 virus in the supernatant revealed that all seven DSGs significantly reduced HCMV virus
443 production with many of DSGs yielding virus concentrations near the limit of detection **(Figure**
444 **7H)**. Consistent with the results from the screen, the effect of DSGs on HSV-1 replication was
445 less pronounced compared to HCMV **(Figure 7I)**. However, MBD3L2, H3Y1, and PRAMEF20
446 reduced HSV-1 virus production by between one and four logarithms. These data show that many
447 DSGs function as antiviral mediators.

448 ## Discussion

449 Placental trophoblasts form the barrier between the maternal and fetal compartments of the
450 MFI and possess cell-autonomous mechanisms of protecting the developing fetus from the
451 vertical transmission of viruses.[1,2] Furthermore, trophoblasts have been shown to restrict the
452 replication of prominent teratogenic herpesviruses such as HCMV.[20,21] In this study, we profiled
453 the response of TOs to seven teratogenic viruses and identified the expression of DUX4 and
454 downstream target DSGs as a unique response to herpesvirus infections. Comparison between
455 TOs and matched maternally-derived DOs revealed that DUX4 and DSGs are induced to
456 significantly higher levels in TOs by both HSV-1 and HCMV, suggesting that it is uniquely induced
457 in trophoblasts. Using scRNAseq and pseudotime trajectory analysis, we identified a unique
458 pathway in HSV-1-infected TOs. This trajectory was distinct from the typical virus replication
459 trajectory and was characterized by the expression of *DUX4* and downstream target DSGs,
460 consistent with this program being antiviral. Overexpression screening of the most highly induced
461 DSGs demonstrated that many of these genes significantly impaired the replication of HSV-1 and
462 HCMV in permissive cells. These findings uncover a previously unrecognized antiviral pathway in
463 human trophoblasts, wherein the induction of DUX4 and its downstream target genes serves as
464 a cell-intrinsic defense mechanism against herpesvirus infections. This discovery highlights the
465 unique antiviral strategies employed by trophoblasts to protect the developing fetus from
466 teratogenic viral threats.

467 A relationship between the DUX4 program and herpesvirus infection has emerged, but there
468 is not a consensus on its role in virus replication. Expression of DUX4 or select DSGs have been
469 observed in response to infection with alpha, beta, and gamma herpesviruses in cell culture as
470 well as in herpesvirus-mediated cancers.[37,54-56] Induction of DUX4 following herpesvirus infection
471 was originally described based on the antiviral activity of the E3 ubiquitin ligase TRIM43.[37]
472 TRIM43 was proposed to impair herpesvirus replication by directing components of the
473 centrosome for degradation leading to destabilization of the nuclear envelope.[37] Recently,

474 knockdown of the DSGs *RASD1* and *RRAD*, which are Ras-related GTPases, was found to
475 augment HSV-1 virion production in fibroblasts.[38] As the above DSGs exert antiviral activity,
476 DUX4 and DSGs have been suggested to be a part of the cell-intrinsic defenses against
477 herpesvirus infection. Contrary to this model, a recent study has shown that HSV-1 and HSV-2
478 replication is impaired in DUX4 KO HAP1 cells and DUX4 knockdown HEK293 cells, suggesting
479 that aspects of the DUX4 program may be coopted by the virus to facilitate replication in some
480 contexts.[56] In a primary cell-derived trophoblast system, we found that the expression of DUX4
481 and the majority of DSGs defined a low viral gene expression trajectory following HSV-1 infection
482 in TOs. Consistent with this, overexpression of the majority of DSGs restricted HSV-1 and/or
483 HCMV replication in MRC5 fibroblasts. Thus, our data support a model in which DSGs are a
484 component of the cell-intrinsic defenses against herpesvirus replication. In the cell types
485 examined in previous studies, DSG induction typically occurs alongside canonical IFN antiviral
486 signaling, which likely serves as the primary antiviral defense mechanism. In contrast, our findings
487 reveal that in human trophoblasts, the DUX4 pathway operates as the predominant defense
488 mechanism against herpesvirus infections, representing a specialized antiviral strategy unique to
489 this cell type. Our data expands our conception of DUX4 and DSGs from isolated antiviral genes
490 controlled by a common transcription factor to a coordinated cell-intrinsic antiviral pathway in
491 human trophoblasts.

492 Most DSGs are not expressed at detectable levels in normal adult cells, and many remain
493 largely uncharacterized. Their specific roles and potential functions are poorly understood,
494 highlighting a significant gap in our knowledge about these genes and their biological importance.
495 Apart from *TRIM43*, *RASD1*, and *RRAD*,[37,38] it remained unclear how many DSGs exert anti-viral
496 activity. Thus, we tested the impact of overexpression of 30 DSGs that were highly expressed in
497 TOs on HSV-1 and HCMV replication in permissive MRC5 cells. Twenty-one of these genes
498 reduced fluorescent protein expression of at least one virus by >50% during at least one timepoint.
499 If we extrapolate to include genes that were excluded based on the >90% peptide identity cutoff,

500 this screen identified 42 novel potentially antiviral human ORFs. Of note, one of the three genes
501 that had little impact on the replication of either virus at any timepoint was *TRIM43*. *RASD1* and
502 *RRAD* were not tested in this screen because they did not meet the expression cutoffs in TOs for
503 inclusion. Additionally, none of the DSGs in the screen led to an increase in viral fluorescent
504 protein expression above that of the control vector. One of the top antiviral DSGs identified by the
505 screen was *CCNA1*, which is a meiosis-specific cyclin A gene in mammals.[57] Although, *CCNA1*
506 has not been previously studied in the context of virus replication, its paralog *CCNA2* restricts
507 HCMV replication.[58] The largest group of genes represented in our screen were the PRAME
508 (preferentially expressed antigen in melanoma) family of leucine-rich repeat proteins. All five of
509 the PRAME family genes tested displayed some level of anti-viral activity, with *PRAMEF2*,
510 *PRAEMF8*, and *PRAMEF20* being among the top hits for both viruses. The only member of this
511 family in humans to have been studied mechanistically is *PRAME*, which can function as a
512 negative regulator of retinoic acid signaling.[59,60] However, *PRAME* does not appear to be a DSG
513 based on our analyses, and involvement in retinoic acid signaling has not been confirmed with
514 any other PRAME family members which share at most 53% peptide identity with *PRAME*. The
515 PRAME family is extensively duplicated in mammals. Additionally, both the PRAME family and
516 *LEUTX*, another top hit from this screen, have high allelic variation in humans and exhibit signs
517 of positive selection, which are common features of antiviral gene families.[61-63] Our findings
518 suggest that herpesvirus infections may have exerted evolutionary selective pressure on the
519 development and retention of these genes. We conclude that many of the highly upregulated
520 DSGs in trophoblasts possess strong anti-herpesvirus activity, positioning them as compelling
521 targets for future mechanistic studies to better understand their roles in antiviral defense and
522 potential therapeutic applications.

523 A detailed mechanism of how herpesvirus infection triggers *DUX4* expression has yet to be
524 reported. A recent study suggests that the HSV-1 immediate early genes RL2 (ICP0) and US1
525 (ICP4) are necessary and sufficient to induce DUX4 expression in HSV-1 infection.[56] In our

526 scRNAseq data of HSV-1 infection in TOs, we observed that 9 out of 50 HSV-1 genes were
527 expressed at comparable or higher levels in the DUX4-high cluster when compared to the HSV-
528 1-high cluster. All of these genes were immediate early (α), early (β), or unclassified HSV-1
529 transcripts. Thus, DUX4 expression being triggered by the activities of one or several immediate
530 early genes may explain this expression pattern. Importantly, US1 was not among the HSV-1
531 genes with higher expression in the DUX4-high cluster and the expression of RL2 was too low to
532 accurately conclude a pattern of expression between these clusters. Another observation that
533 may point to how DUX4 is controlled is that TOs respond to HCMV and HSV-1 with much higher
534 expression of both *DUX4* and downstream DSGs than matched maternal DOs. As trophoblasts
535 uniquely constitutively secrete IFN-λs,[12,18-20] we hypothesized that constitutive type-III IFN
536 signaling may modulate *DUX4* and DSG expression. However, knock-out of *IFNLR1* did not
537 decrease *DUX4* or DSG expression in TOs following HSV-1 infection, demonstrating that
538 constitutive type III IFN signaling does not influence this pathway. Nonetheless our data indicate
539 that TOs respond to herpesvirus infection with uniquely high expression of *DUX4* and DSGs,
540 which could be used in future studies to investigate how this pathway is induced and modulated
541 during herpesvirus infection.

542 Immune responses at the MFI must be tightly regulated to prevent damage to the developing
543 fetus. For example, in mice the type I IFN response, either induced by viruses or poly I:C, can
544 cause placental damage and lead to fetal demise.[14-16,64] Although RuV infection induced IFN and
545 ISG expression in TOs, demonstrating that IFN pathways can be activated in this model, HSV-1,
546 HSV-2, and HCMV infection had minimal impact on the expression of IFNs and ISGs. The
547 induction of DSGs may also have potential negative impacts on trophoblast function, raising the
548 possibility of trade-offs between antiviral defense and maintaining normal cellular processes.
549 Expression of DUX4 and six of the DSGs that were tested in our screen led to cell death in MRC5
550 cells, suggesting that expression of these genes could also be lethal in trophoblasts. Additionally,
551 although scRNAseq analysis of iDUX4 expression and HSV-1 infection revealed that all

552 trophoblast cell types can produce DSGs, the STB was one of the clusters that expressed the
553 highest levels of DSGs in response to HSV-1 infection. The STB is a critical trophoblast cell type
554 that participates in placental hormone secretion and nutrient, gas, and waste exchange. The
555 impacts of expression of a potently lethal gene in a polynuclear fused cell such as the STB are
556 unclear. DUX4 causes FSHD when aberrantly expressed in adult muscle cells—another
557 polynuclear fused cell type.[35,36] Finally, many DSGs are small molecule transporters, such as the
558 sodium phosphate transporter *SLC34A2* and the amino acid transporter *SLC36A2,*[65,66] which
559 were induced by 240-fold and 11-fold respectively by iDUX4 expression in TOs. In MRC5 cells
560 expression of SLC34A2 had a small impact on HCMV replication at one timepoint and no impact
561 on HSV-1 replication. However, an increase in expression of small molecule transporters could
562 disrupt the crucial functions of nutrient and waste exchange between the maternal and fetal blood
563 supplies across the STB. Thus, our data present the possibility that DUX4 expression in
564 trophoblasts following herpesvirus infection could contribute to impaired placental function.

565 The data presented here establish that DUX4 and its transcriptional targets, termed DSGs,
566 form the central response mechanism of trophoblasts to herpesvirus infection, underscoring their
567 critical role in the antiviral defense of these specialized cells. Like ISGs, DSGs are induced as
568 part of an antiviral defense mechanism and encode non-redundant effectors that likely target
569 distinct aspects of viral replication. However, the DUX4-DSG pathway appears uniquely adapted
570 for pregnancy, enabling a cell-intrinsic antiviral response in trophoblasts without activating
571 paracrine signaling that could disrupt maternal immune tolerance. Given the high prevalence of
572 herpesvirus exposure during pregnancy, this pathway may have evolved to balance effective
573 antiviral defense with the preservation of placental function and immune tolerance, ensuring
574 optimal pregnancy outcomes. These insights not only deepen our understanding of trophoblast
575 biology but also open new avenues for exploring therapeutic strategies to protect against
576 teratogenic viral infections.

Acknowledgements

This work was supported by NIH grants F32-AI183633 (JH), R01-AI173333 (CC), P01-AI129859 (CC), and R01-AI145828 (CC). We would like to acknowledge Phillip Kolb (University Hospital Freiburg), Rebecca Göttler (University Hospital Freiburg), Nat Moorman (University of North Carolina at Chapel Hill) and Bekah Dickmander (University of North Carolina at Chapel Hill) for assistance with HCMV propagation.

584 ## Materials and Methods

585 **Culture of trophoblast and decidua organoids.**

586 TO and DO lines employed in this study were derived from full-term placental tissue as
587 previously described.[20,67,68] Human tissue used in this study was obtained from Duke University
588 after approval from the Duke University Institutional Review Board and in accordance with the
589 guidelines of Duke University human tissue procurement. TOs were cultured by plating in domes
590 of Matrigel (Corning 356231) and maintained with term trophoblast organoid medium (tTOM)
591 [Advanced DMEM/F12 (Life Technologies, 12634010) supplemented with 1X B27 (Life
592 Technologies, 17504044), 1× N2 (Life Technologies, 17502-048), 10% FBS (vol/vol, Cytiva
593 HyClone, SH30070.03), 2 mM GlutaMAX™ supplement (Life Technologies, 35050061), 100
594 µg/ml Primocin (InvivoGen, ant-pm-1), 1.25 mM N-acetyl-L-cysteine (Sigma, A9165), 500 nM
595 A83-01 (Tocris, 2939), 1.5 µM CHIR99021 (Tocris, 4423), 50 ng/ml recombinant human EGF
596 (Gibco, PHG0314), 80 ng/ml recombinant human R-spondin 1 (R&D systems, 4645-RS-100), 100
597 ng/ml recombinant human FGF2 (Peprotech, 100-18C), 50 ng/ml recombinant human HGF
598 (Peprotech, 100-39), 10 mM nicotinamide (Sigma, N0636-100G), 5 µM Y-27632 (Sigma, Y0503-
599 1MG) and 2.5 µM prostaglandin E2 (PGE2, Tocris, 2296)].[20] DOs were maintained in Expansion
600 Medium (ExM) [Advanced DMEM/F12 (Life Technologies, 12634010) supplemented with 1X B27
601 without vitamin A (Life Technologies, 12587010), 1× N2 (Life Technologies, 17502-048), 2 mM
602 GlutaMAX™ supplement (Life Technologies, 35050061), 100 µg/ml Primocin (InvivoGen, ant-pm-
603 1), 1.25 mM N-acetyl-L-cysteine (Sigma, A9165), 500 nM A83-01 (Tocris, 2939), 50 ng/ml
604 recombinant human EGF (Gibco, PHG0314), 100 ng/mL recombinant human Noggin (Peprotech,
605 120-10C), 80 ng/ml recombinant human R-spondin 1 (R&D systems, 4645-RS-100), 100 ng/ml
606 recombinant human FGF-10 (Peprotech, 100-26), 50 ng/ml recombinant human HGF (Peprotech,
607 100-39), 10 mM nicotinamide (Sigma, N0636-100G), and 2.5 µM Y-27632 (Sigma, Y0503-
608 1MG)].[68] Organoid cultures were maintained in a humidified incubator with 5% CO_2 at 37°C, and
609 medium was renewed every 2-3 days. After 4-5 days in culture, organoids were grown in their

610 respective growth media without Y-27632. Organoids were passaged after 5-7 days in culture by
611 collecting Matrigel domes, digesting with TrypLE Express (Gibco, 12605-028) for 6-12 min at 37°C,
612 then mechanically dissociating into single cells and small fragments by manual pipetting.
613 Resulting cells were resuspended in Matrigel and plated as domes in 24-well tissue culture plates.
614

615 **Culture of cell lines and viruses.**

616 Lenti-X™ 293T cells (Takara, 632180), ARPE-19 cells (ATCC, CRL-2302) and Vero (ATCC,
617 CCL-81) cells were cultured in Dulbecco's minimal essential medium (DMEM) with 10% FBS and
618 1% penicillin/streptomycin (Gibco, 15140). MRC5 cells (ATCC, CCL-171) were cultured in DMEM
619 with 10% FBS, 1% penicillin/streptomycin (Gibco, 15140), 1x HyClone™ non-essential amino
620 acids (Cytiva, SH30238.01), 1 mM sodium pyruvate (Cytiva, SH30239.01). Cell lines were tested
621 for mycoplasma using the MycoStrip Mycoplasma Detection Kit (Invivogen, rep-mys-50).

622 mCherry-tagged HCMV TB40/E (a gift from N. Moorman[69]) was propagated by infecting ARPE-
623 19 (MOI ≅ 0.01) followed by extended incubation until >90% of cells showed CPE. Growth on
624 ARPE-19 cells was chosen to select for epithelial tropism. Both supernatant and cells were
625 harvested, cells were gently lysed by freeze/thaw, and pooled cell-associated and cell-free virus
626 was concentrated on a 20% sucrose cushion (20,000 rpm). Virus pellet was the resuspended in
627 sterile media before titration on MRC5 cells and ARPE-19 cells. The remaining virus stocks were
628 previously prepared, and aliquots were pulled from storage at -80°C for experiments. GFP-UL25
629 HSV-1 KOS strain (a gift from F. Homa[70]),[11] HSV-2 333 strain (a gift from H. Lazear), YFP-tagged
630 VACV Western Reserve strain (a gift from S. Cherry),[11] RuV M33 strain (ATCC, VR-315),[71] and
631 ZIKV Paraiba-2015 strain (a gift from D. Watkins)[12] were all titrated on Vero cells. Echo5 Noyce
632 strain was titrated on HeLa cells [72].
633

634 **Virus infection in organoids**

635 Virus infections in organoids were performed either on coat-seeded cultures or in suspension.
636 Matrigel coats were generated by covering the bottom of a 48-well plate or 8-well chamber slide
637 with 20 uL of undiluted Matrigel, which was then allowed to polymerize for ~10 min. Dissociated
638 organoids were seeded on Matrigel coats following passage and allowed to grow in for 5-7 days
639 prior to infection. The coat-culturing method allows organoids to grow into 3D spherical structures,
640 but leaves the majority of the surface of each organoid unit exposed to the media rather than fully
641 imbedded in matrigel as is typical in Matrigel domes. Coat-seeded organoids were infected by
642 replacing the culturing media with inoculum (virus diluted in tTOM), incubating for 2 h at 37°C,
643 and then replacing the inoculum with fresh culturing media. Suspension infections were performed
644 by first releasing organoids from Matrigel domes using cell recovery solution (Corning, 354253)
645 at 4°C for 20-30 min. Organoids were pelleted by gravity, washed with PBS, and pelleted again.
646 Inoculum was then added to the released organoids. Infections were allowed to proceed for 2 h
647 at 37°C, agitating the culture every 30 min to keep the organoids from aggregating. Organoids
648 were then pelleted, resuspended in Matrigel, seeded in domes in 24-well plates, and submerged
649 with normal tTOM. Prior to infections, parallel wells of organoids were disrupted and counted to
650 calculate MOI. MOI for each experiment is specified in the results and figure legends.
651
652 **Lentivirus production.**
653 Lentiviral particles were produced in Lenti-X™ 293T cells (Takara, 632180) by transfection of
654 a lentiviral transfer plasmid along with psPAX2 (Addgene #12260) and pMD2.G (Addgene #12259)
655 packaging plasmids using TransIT®-293 transfection reagent (Mirus Bio, MIR 2700). 293T cells
656 were refed with intended target cell medium at 24 h post transfection. Supernatant was collected
657 at 48 h post transfection, filtered with 0.45 µm filter, then stored at -80°C prior to transduction of
658 target cells. psPAX2 and pMD2.G were gifts from Didier Trono. pCW57.1-DUX4-CA, used to
659 generate iDUX4 lentiviral particles, was a gift from Stephen Tapscott (Addgene #99281).[45]
660 Lentiviral plasmids for the overexpression of DSGs, CRISPR-Cas9-mediated editing of IFNLR1,

661 shRNAs, CRISPRi, and dominant-negative DUX4 overexpression were constructed by
662 VectorBuilder. Descriptions of these vectors along with vector IDs (that can be used to retrieve
663 detailed information on them) can be found in **Table S7**.
664
665 **Transduction and single-cell cloning of trophoblast organoids.**
666 Trophoblast organoids were transduced by first dissociating them into single-cell suspension
667 following the same protocol for passaging described above. The dissociated single cell
668 suspension was then incubated with filtered lentiviral supernatant and 8 µg/mL polybrene
669 overnight in an ultralow attachment plate at 37°C overnight. The transduced cell suspension was
670 resuspended in Matrigel and plated as domes. After 2-3 days of recovery, transduced cells were
671 selected for by supplementing the media with 2 ug/mL puromycin for 4-5 days. Single cell clones
672 of CRISPR-Cas9-edited organoids were generated by isolating and propagating individual
673 organoid units one passage after selection. This process takes advantage of the likelihood that
674 most organoids in Matrigel arise from a single or very few starting stem cells. Clonal organoid
675 lines were screened for knockout by isolating genomic DNA using GenElute Mammalian Genomic
676 DNA Purification Kit (Sigma, G1N350), amplifying the sgRNA target region using high-fidelity PCR,
677 and the sequencing the purified PCR product with sanger sequencing at GENEWIZ. The resulting
678 capillary electrophoresis traces were analyzed using the ICE analysis tool from Synthego. The
679 primers used to amplify the sgRNA target editing site in *IFNLR1* are listed in **Table S7**.
680
681 **Immunofluorescence, confocal microscopy, and confocal image analysis.**
682 For immunofluorescence staining, organoids cultured in a layer of matrigel on 8-well chamber
683 slides. Organoids were fixed with 4% paraformaldehyde for 30 min, permeabilized with PBS with
684 0.5% Triton X-100 for 60 min, then blocked with 10% normal goat serum in PBS with 0.05%
685 TWEEN-20 for 60 min. Organoids were then incubated with primary antibody diluted in blocking
686 solution at 4°C overnight. Organoids were then washed with PBS and then incubated for 2 hr at

687 room temperature with Alexa Fluor-conjugated secondary antibodies. Organoids were washed
688 again with PBS and mounted in Vectashield (Vector Laboratories) containing 4′,6-diamidino- 2-
689 phenylindole (DAPI). The following antibodies were used for staining: DUX4 (Sigma, MABD116),
690 anti-V5-tag (Cell Signaling Technologies, #58009), Alexa Fluor 488 Goat anti-Mouse IgG
691 secondary antibody (Invitrogen, A11029), and Alexa Fluor 594 Goat anti-Rabbit IgG secondary
692 antibody (Invitrogen, A11037). Images were captured on an Olympus Fluoview FV3000 laser
693 scanning confocal microscope.

694 Nuclear mean gray value (MGV) measurements were calculated using an ImageJ macro that
695 first runs the StarDist package on images from the DAPI channel to generate individual regions
696 on interest (ROIs) for every nucleus.[73] These ROIs are then applied to images from other channels
697 to measure there MGVs within each nucleus.

698

699 **Overexpression screen and automated microscopy.**

700 Lentivirus particles for constructs used in the screen were prepared as described above and
701 arrayed into 96-well plate format for this screen. MRC5 cells were seeded into 96-well plate format
702 at a density of 5 x 10^3 cells per well. The following day, the media on these cells was replaced
703 with MRC5 culturing medium supplemented with 16 µg/mL polybrene. 100 µL of the appropriate
704 lentivirus or mock media was added to each well. Transductions were performed in triplicate.
705 Transduction plates were then incubated statically at 37°C for 30 min, centrifuged at 800xg for 30
706 min, then incubated for an additional hour statically at 37°C. Transduction media was then
707 replaced with fresh culturing media. 24 h post transduction, the media was replaced with MRC5
708 culturing media supplemented with 2 µg/mL puromycin, and selection was allowed to proceed for
709 48 h. 72 h post transduction, selected cells were infected with HCMV TB40/E mCherry (5 x 10^4
710 particles/well), HSV-1 KOS GFP (5 x 10^3 particles/well), or mock media. Inoculums were applied
711 to cells for 2 h statically at 37°C. Inoculum was then replaced with fresh media. A Keyence BZ-
712 X810 all-in-one automated microscope was used to capture fluorescent and bright field images

713 at 10x magnification of every well at 24 h intervals for the duration of each experiment. Five fields
714 of images were captured per well. Cultures were maintained in a humidified, 37°C chamber during
715 imaging. Lentiviral constructs that led to complete cell death were excluded from further analysis.
716 This was defined by visual morphological assessment of bright field images (spherical cell body
717 and/or detachment) at 0 hpi and 24 hpi, which are timepoints at which CPE is not observed by
718 either virus in control conditions. Fluorescence quantification was performed using BZ-X800
719 Image Analyzer (Keyence). Cell body areas were defined algorithmically using brightfield images.
720 Fluorescence intensity of the virally encoded tags were integrated within these areas and then
721 normalized to the total cellular area (in μm^2), yielding an RFU / μm^2 measurement for each well
722 at each timepoint.
723
724 **Virus titration assays**
725 HCMV infectious virus was quantified by focus-forming assay. Briefly, supernatants from
726 HCMV replication experiments were serially diluted, and used to infect MRC5 cells. At 4 dpi, these
727 cells were fixed in 2% paraformaldehyde for 1 h. Cells were then stained for HCMV gene
728 expression by permeabilizing with PBS containing 0.5% Triton X-100 and 1% BSA for 20 min.
729 Cells were then incubated overnight at 4°C with an anti-UL44 primary antibody (Virusys, CA006-
730 100) at a 1:5000 dilution in PBS containing 0.1% TWEEN20 and 1% BSA. Cells were then washed
731 and counter-stained for > 1 h at room temperature with anti-mouse IgG-HRP (Bio-Rad, #1706516)
732 diluted 1:2000 in PBS containing 0.1% TWEEN20 and 1% BSA. Cells were then incubated with
733 DAB (3,3'Diaminobenzidine) chromogen (Abcam, ab64238) following the manufactures
734 instructions. UL44-positive cells at the most dilute sample with detectable staining were counted
735 and used to calculate focus-forming units (FFU) per mL (FFU/mL). HSV-1 infectious virus was
736 quantified using the 50% tissue culture infectious dose (TCID50) method. Briefly, supernatants
737 from HSV-1 replication experiments were serially diluted and used to infect Vero cells. At 7 dpi,
738 cells were fixed and stained simultaneously with a crystal violet solution in PBS containing 2%

739 PFA. The number of wells with detectable monolayer disruption at each dilution were counted
740 and used to calculate TCID50/mL.
741
742 **RNA extraction, qRT-PCR, and bulk RNAseq**
743 RNA for qRT-PCR and bulk RNAseq was purified using the Sigma GenElute total mammalian
744 RNA miniprep kit or the Qiagen RNAeasy Mini Kit following the manufacturer's instruction. cDNA
745 for qRT-PCR was generated from total RNA using iScript cDNA synthesis kit (Bio-Rad) following
746 the manufacturer's instructions. Quantitative PCR was performed using the iQ SYBR Green
747 Supermix (Bio-Rad, 1708882) on a CFX96 Touch Real-Time PCR Detection System (Bio-Rad).
748 Gene expression was determined based on a ΔCT method normalized to actin. Primers used for
749 qPCR can be found in **Table S7**.
750 Bulk RNAseq libraries were prepared by the Duke Center for Genomic and Computational
751 Biology using the KAPA mRNA HyperPrep Kit (Roche). Sequencing was performed as follows:
752 on a NovaSeq X Plus using 100 bp paired end sequencing for the diverse virus TO infection
753 experiment, on a NovaSeq 1000 using 100 bp paired end sequencing for the iDUX4 experiment,
754 and on a NextSeq 500 using 75 by paired end sequencing for the HSV-1 infection in matched TO
755 and DO experiment. The following datasets were downloaded from Sequence Read Archive (SRA)
756 and used in analyses: TO/DO infections with HCMV TB40/E and HCMV AD169r
757 (PRJNA869760),[20] TSC infections with HCMV TB40/E (PRJNA1045985),[21] iDUX4 expression in
758 iPSCs (PRJNA377314),[34] and iDUX4 expression in MB135 cells (PRJNA338591).[45]
759 RNAseq reads were aligned to the human genome (GRCh38) and the appropriate viral
760 genomes for each experiment using QIAGEN CLC Genomics Workbench (v24). Viral genomes
761 used in mapping are as follows: HCMV TB40/E (GenBank: MW439039.1), HSV-1 KOS (GenBank:
762 KT899744.1), HSV-2 333 (GenBank: LS480640.1), VACV WR (GenBank Assembly:
763 GCA_000860085.1), Echo5 Noyce (GenBank: AF083069.1), RuV M33 (GenBank: OM816674.1),
764 and ZIKV Paraíba (GenBank: KX280026.1). Differential gene expression analysis was performed

765 using DESeq2 package in R accounting for multiple donors in the statistical model.[39] PCA analysis
766 was performed using PCAtools package in R following correction for donor, experimental set, and
767 dpi batch effects using the ComBat function of the sva package.[74] Heatmaps were generated
768 using $\log_2$ normalized counts (an output from DESeq2) and the pheatmap package in R. Raw
769 data from the bulk RNAseq experiments reported here have been deposited into SRA
770 (PRJNA1213838).
771
772 **Dissociation of organoids for single cell RNAseq.**
773 Matrigel domes of organoids were resuspended into media [Advanced DMEM/F12 (Life
774 Technologies, 12634010) supplemented with 1% penicillin/streptomycin (Gibco, 15140), 10 mM
775 HEPES (Gibco, 15630-106), and 2 mM GlutaMAX™ supplement (Life Technologies, 35050061)]
776 and organoids were pelleted by centrifugation. The media was replaced by TrypLE Express
777 (Gibco, 12605-028), and organoids were digested at 37°C for 12 min. Organoids were pelleted
778 again and resuspended in 200 uL resuspension media and vigorously disrupted by manual
779 pipetting (~180 pipettes per min) for 3 min. The volume of the cell suspension was increased to 1
780 mL with PBS supplemented with 1% FBS. The cell suspension was then filtered through a 40 µm
781 filter cell strainer (Corning, 352098) using an additional 3 mL of PBS supplemented with 1% FBS
782 to wash the filter. Cells were pelleted by centrifugation and resuspended in 100 µL of PBS
783 supplemented with 1% FBS. Cells were counted and viability tested using trypan blue and
784 automated cell counting (Biorad TC20 automated cell counter). All samples had >1 x 10^6 live
785 cells/mL and viabilities >70%.
786
787 **Single-cell RNAseq library preparation and data analysis.**
788 Libraries were prepared from ~10,000 cells using 10x Genomics Single Cell 3' reagent kits (v2
789 chemistry, #CG00052) on a Chromium X instrument (10x Genomics) by the Molecular Genomics
790 Core at the Duke Molecular Physiology Institute. Sequencing was performed on a NovaSeq X

791 sequencer using a S4 flow cell which was predicted to yield around 71k reads / cell. Custom
792 genomes were constructed using the CellRanger package (v6.1.2, 10x Genomics) in Linux by
793 adding either the iDUX4 lentiviral vector sequence or the HSV-1 KOS genome (GenBank:
794 KT899744.1) to the human genome (GRCh38) as additional chromosomes. HSV-1 genes that
795 share a polyadenylation site (e.g. polycistronic or alternatively spliced transcripts) were grouped
796 into single features as they cannot be distinguished by the employed library preparation chemistry.
797 Post-processing and read alignment to these custom genomes were performed using the 10x
798 CellRanger package hosted through the 10x cloud analysis platform. Gene expression matrices
799 were analyzed using the Seurat (version 4) package in R.[75] Cells with between 2000 and 12000
800 uniquely expressed genes and between 4% and 25% mitochondrial reads were included for
801 downstream analysis. To eliminate batch effects, samples from different donors within the same
802 condition were normalized and integrated using the SCTransform and FindIntegrationFeatures
803 functions in Seurat while simultaneously regressing the following variables: percent mitochondrial
804 reads, percent ribosomal reads, percent X chromosome reads, percent Y chromosome reads,
805 number of features per cell, number of counts per cell, and percent HSV-1 reads (for the HSV-1
806 infection dataset) or DUX4/DSG score (for the iDUX4 dataset). The RNA assay was scaled and
807 normalized and ALRA-mediated imputation of the data was performed before subsequent
808 analyses.[76] Samples from separate conditions were then merged together using the Harmony
809 package in R.[77] Dimensional reduction was performed using the RunPCA function followed by the
810 RunUMAP function using the top 50 principle component dimensions. The FindNeighbors and
811 FindClusters commands were used to perform clustering at a resolution of 0.6. Determination of
812 an optimal resolution was aided by the clustree package.[78] Correlation between iDUX4 and all
813 other genes was performed using the Pearson correlation setting of the base cor() function in R.
814 Differential gene expression analysis was performed by retrieving the raw counts from each
815 cluster separated by original sample using the AggregateExpression function and then performing

816 DESeq2 analysis accounting for multiple donors in the statistical model.[39] HSV-1 transcripts were
817 classified as described in Dremel et al.[79]

818 To perform trajectory analysis of HSV-1 infected cells, the data were reanalyzed to only include
819 infected cells and to allow these cells to be ordered based on HSV-1 gene expression. Cells with
820 between 2000 and 12000 uniquely expressed genes, >10000 total reads, between 4% and 25%
821 mitochondrial reads, and >0.1% HSV-1 reads were included for downstream analysis. To
822 eliminate batch effects, samples from different donors were normalized and integrated using the
823 SCTransform and FindIntegrationFeatures functions in Seurat while simultaneously regressing
824 percent X chromosome reads, percent Y chromosome reads, and number of counts per cell.
825 Dimensional reduction was performed using the RunPCA function followed by the RunUMAP
826 function using the top 20 principle component dimensions. The FindNeighbors and FindClusters
827 commands were used to perform clustering at a resolution of 0.6. The SlingShot package in R
828 was used to predict pseudotime orders of infected cells from clusters identified in Seurat using a
829 defined starting cluster and undefined end clusters.[48] The fitGAM function of the tradeSeq
830 package in R was used to fit variable features, HSV-1 genes, and DSGs to a generalized additive
831 model along the predicted pseudotime trajectories.[80] The predictSmooth function was used to plot
832 the average expression of genes in cells along trajectories.

833 Raw data from the scRNAseq experiments reported here have been deposited into SRA
834 (PRJNA1213838).

835

836 **Statistics and reproducibility.**

837 All primary organoid-based experiments in this report have been replicated using independent
838 samples from organoid lines derived from multiple donors. Experiments in cell lines and cloned
839 organoids lines were performed with triplicate independent samples. Data in bar charts are
840 presented as mean ± SD. In all graphics, each individual data point is shown when possible.
841 Statistical significance was determined as described in the figure legends. All statistical analyses

842 were performed using GraphPad Prism, unless otherwise specified (e.g. bulk RNAseq and
843 scRNAseq). Unless otherwise specified, p values of <0.05 were considered to be statistically
844 significant.
845

Figures and Legends

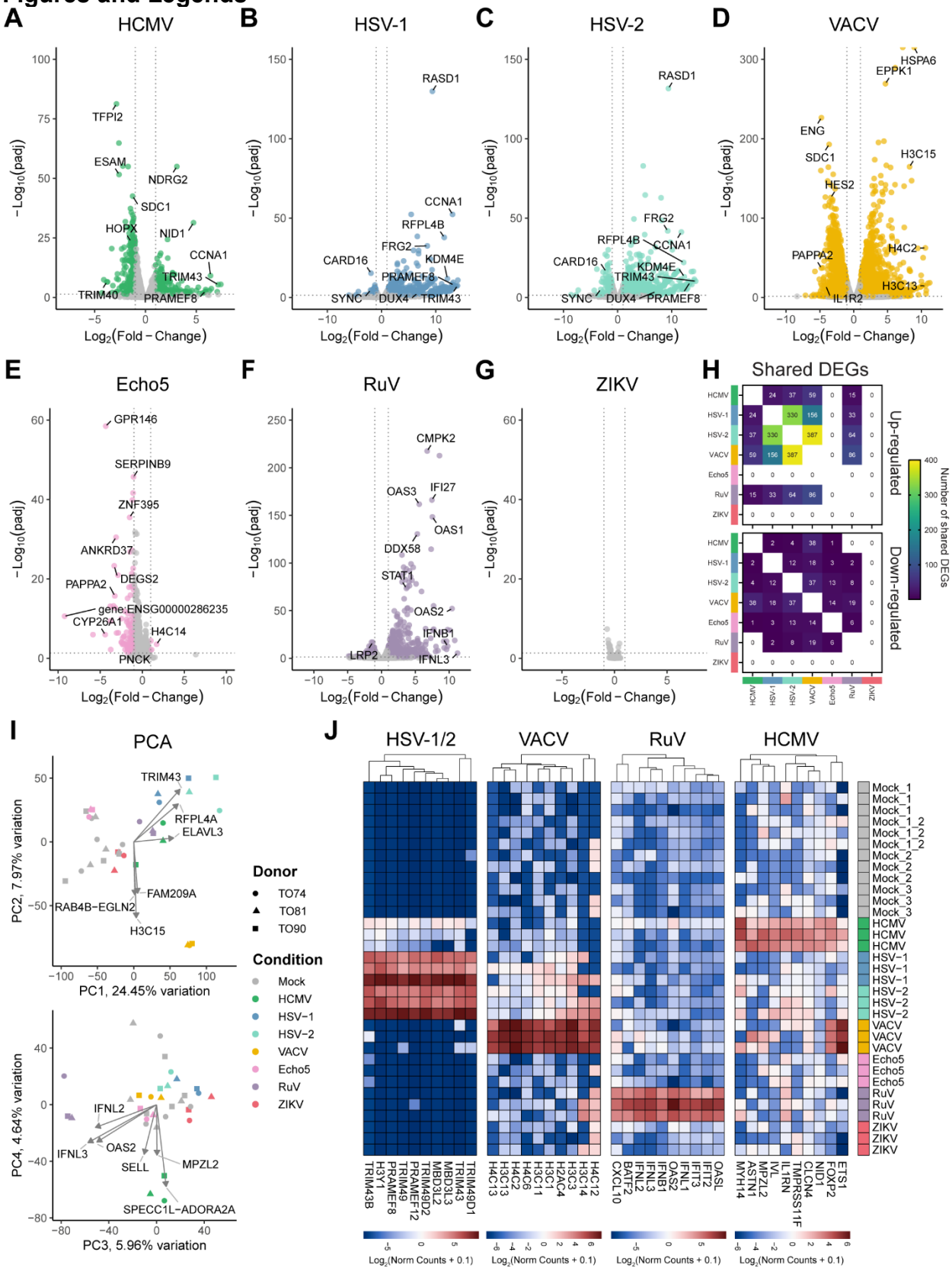

848 **Figure 1 | Trophoblast organoids respond distinctly to diverse viruses.** Trophoblast
849 organoids from three donors were infected with HCMV, HSV-1, HSV-2, VACV, Echo5, RuV, and
850 ZIKV at an MOI of 2. VACV and Echo5 infections were performed in suspension on organoids
851 released from matrigel that were re-imbedded in matrigel following inoculation. All other infections
852 were performed on spherical organoids grown on matrigel coats. mRNA was purified and
853 analyzed by bulk RNAseq. **(A-G)** Volcano plots portraying the DEGs relative to mock samples.
854 Colored circles represent significant DEGs (Log2(fold-change) > 1 and adjusted *p*-value < 0.05).
855 Gray circles represent genes whose expression was not significantly impacted. Also see **Table**
856 **S1**. **(H)** Heatmap showing the number of shared DEGs between each infection condition. Genes
857 that were found to be differentially expressed between donors, timepoints, or experimental sets
858 in the mock infected samples were excluded from these tallies. **(I)** PCA of RNAseq data from each
859 sample is portrayed in two graphs: principle component 1 (PC1) vs PC2 (top) and PC3 vs PC4
860 (bottom). Shapes denote the donor a sample came from, and color denotes the infection condition
861 of the sample. **(J)** Heatmaps portraying the genes that define the responses unique to virus types.
862 Values are $\log_2$ normalized counts from DESeq2 analysis plus a pseudo count of 0.1. Keys are
863 at the bottom of each chart. The scale is not constant between each heatmap. Red indicates
864 higher expression and blue indicates lower expression. Hierarchical clustering of genes is shown
865 at the top.
866

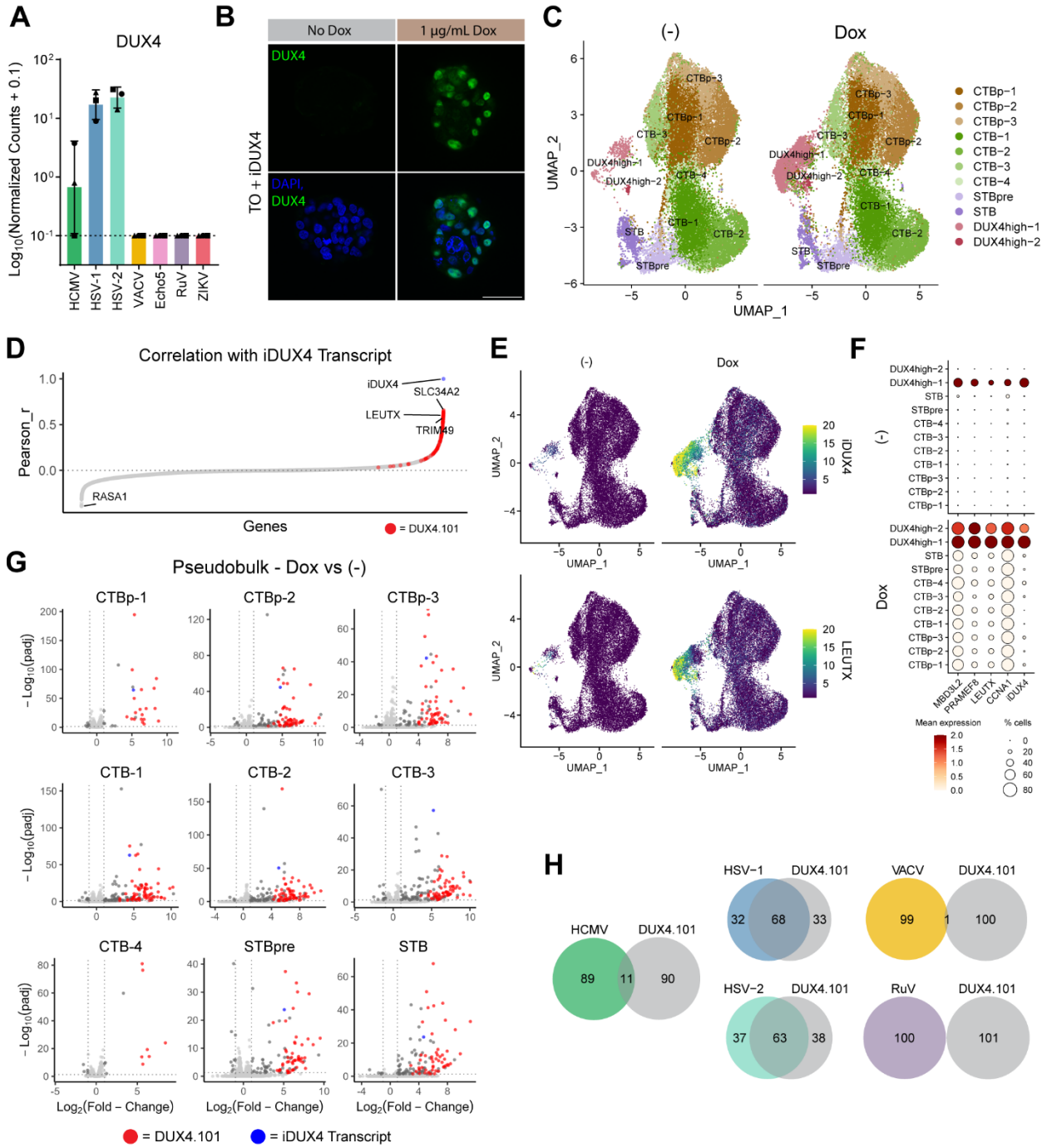

Figure 2 | Trophoblasts respond to herpesviruses with DUX4-stimulated genes. (A) Bar plot portraying the expression of *DUX4* in the RNAseq experiments from Figure 1. Shapes denote the donor of each data point. **(B)** Confocal micrographs of TOs engineered to express DUX4 under a doxycycline (Dox) inducible promoter. DUX4 is displayed in green and DAPI-stained nuclei are in blue. Scale bar = 100 µm. **(C)** UMAP of clusters from three donors of mock-treated TOs and three donors of Dox-treated TOs. Clusters are labeled as proliferative cytotrophoblasts (CTBp), cytotrophoblasts (CTB), pre-syncytiotrophoblasts (STBpre), syncytiotrophoblasts (STB), or DUX4-high cells. Multiple clusters from a single cell type are annotate with a -number after the cluster name. **(D)** Plot portraying the correlation (Pearson's r) between iDUX4 transcript and all

other measured genes. Values are plotted in rank order. Genes that belong to the DUX4.101 list are displayed as red circles. Also see **Table S2**. **(E)** Feature plots of iDUX4 (top) and the *LEUTX* (bottom) expression. Keys are shown to the right. **(F)** Dot plots showing the average expression (ALRA assay) and proportion of cells expressing selected DSGs and iDUX4 in each cluster separated into mock-treated samples (top) and Dox-treated samples (bottom). **(G)** Pseudobulk analysis identifying significant DEGs (Log2(fold-change) > 1 and adjusted *p*-value < 0.05) between Dox-treated samples and mock-treated samples. Results from all clusters other than the DUX4-high clusters are shown. Genes that belong to the DUX4.101 list are displayed as red circles and iDUX4 transcript is displayed as a blue circle. Also see **Table S4**. **(H)** Venn diagrams denoting the overlap between the top 100 DEGs upregulated by each virus and the DUX4.101 list.

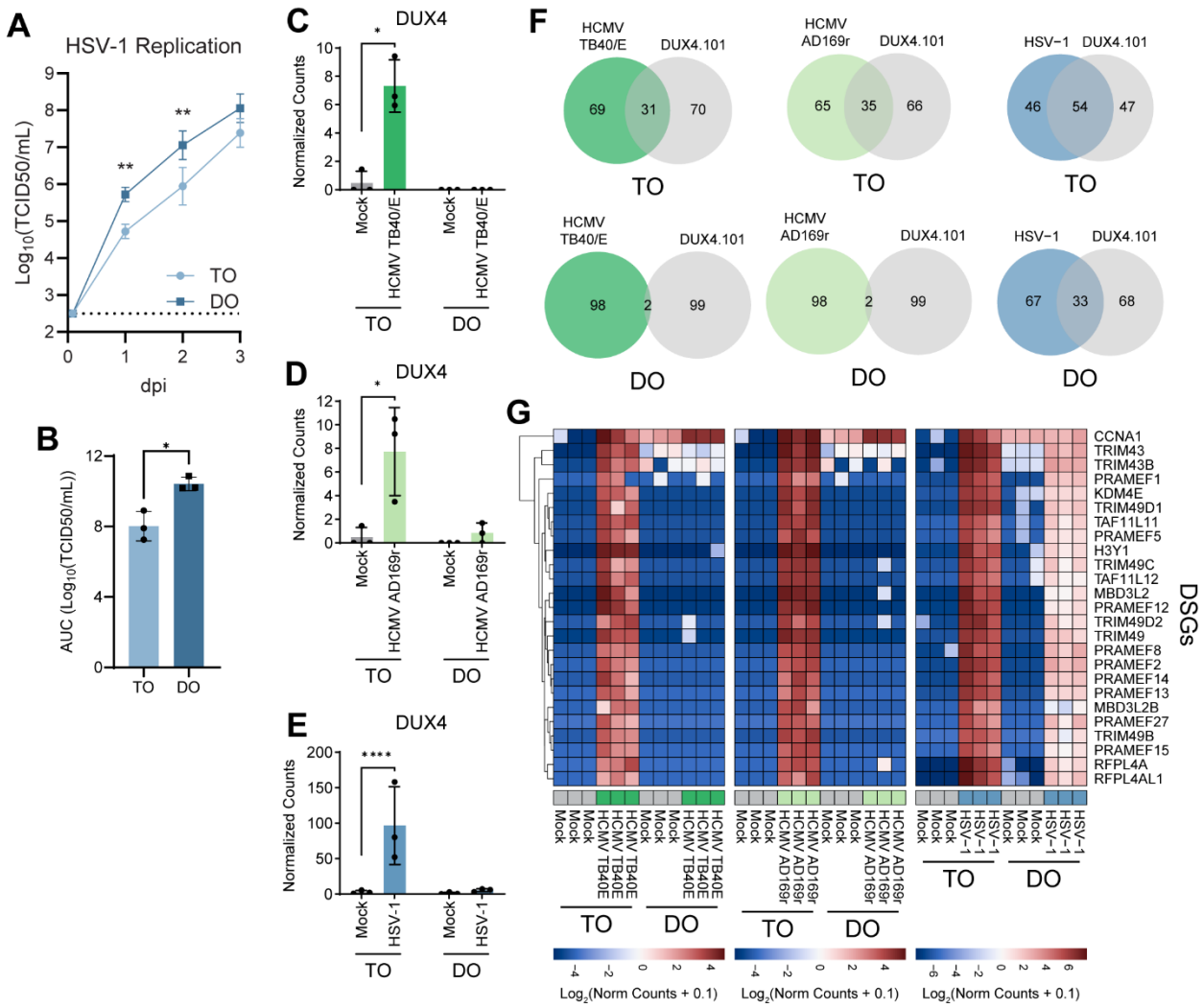

Figure 3 | DUX4-stimulated genes are induced to higher levels in trophoblast organoids than maternal-derived decidua epithelial organoids. (A-B) TOs and DOs were seeded on matrigel coats and infected with HSV-1 at an MOI of 0.1. Infectious HSV-1 particles were quantified using the 50% tissue culture infectious dose (TCID50) method at 2 hpi as well as 1, 2, and 3 dpi (A). Graph displays the mean ± SD at each timepoint. Statistical significance was calculated using 2-way ANOVA, independent t-tests for each timepoint, and the Šidák correction for multiple comparisons. Area under the curve (AUC) was calculated for each independent series of samples (B). Each individual data point is displayed. Bar graph displays the mean ± SD. Statistical significance was determined using by t-test. **(C-G)** HSV-1 infections were performed in suspension on organoids released from matrigel and subsequently re-imbedded in matrigel. RNAseq analysis was employed to assess if TOs and DOs differentially express DUX4 or DSGs when infected with HCMV TB40/E, HCMV AD169r, and HSV-1 (MOI of 5). Also see **Table S5**. **(C-E)** Bar plots portraying the expression of *DUX4* in TOs and DOs in mock-treated samples or those infected with HCMV TB40/E (C), HCMV AD169r (D), and HSV-1 (E). Each individual normalized count value is displayed. Bars represent mean ± SD. Statistical significance was determined using DESeq2 differential expression analysis. **(F)** Venn diagrams denoting the overlap between the top 100 DEGs upregulated by each virus and the DUX4.101 list with TO infections on the top and DO infections on the bottom. **(G)** Heatmaps portraying the expression of canonical DSGs following infection of TOs and DOs with HCMV TB40/E, HCMV AD169r, and HSV-1. Values are $\log_2$ normalized counts from DESeq2 analysis plus a pseudo count of 0.1.

Keys are at the bottom of each chart. The scale is not constant between each heatmap. Red indicates higher expression and blue indicates lower expression. Hierarchical clustering of genes is shown on the left. * $p < 0.05$, ** $p < 0.1$, **** $p < 0.0001$.

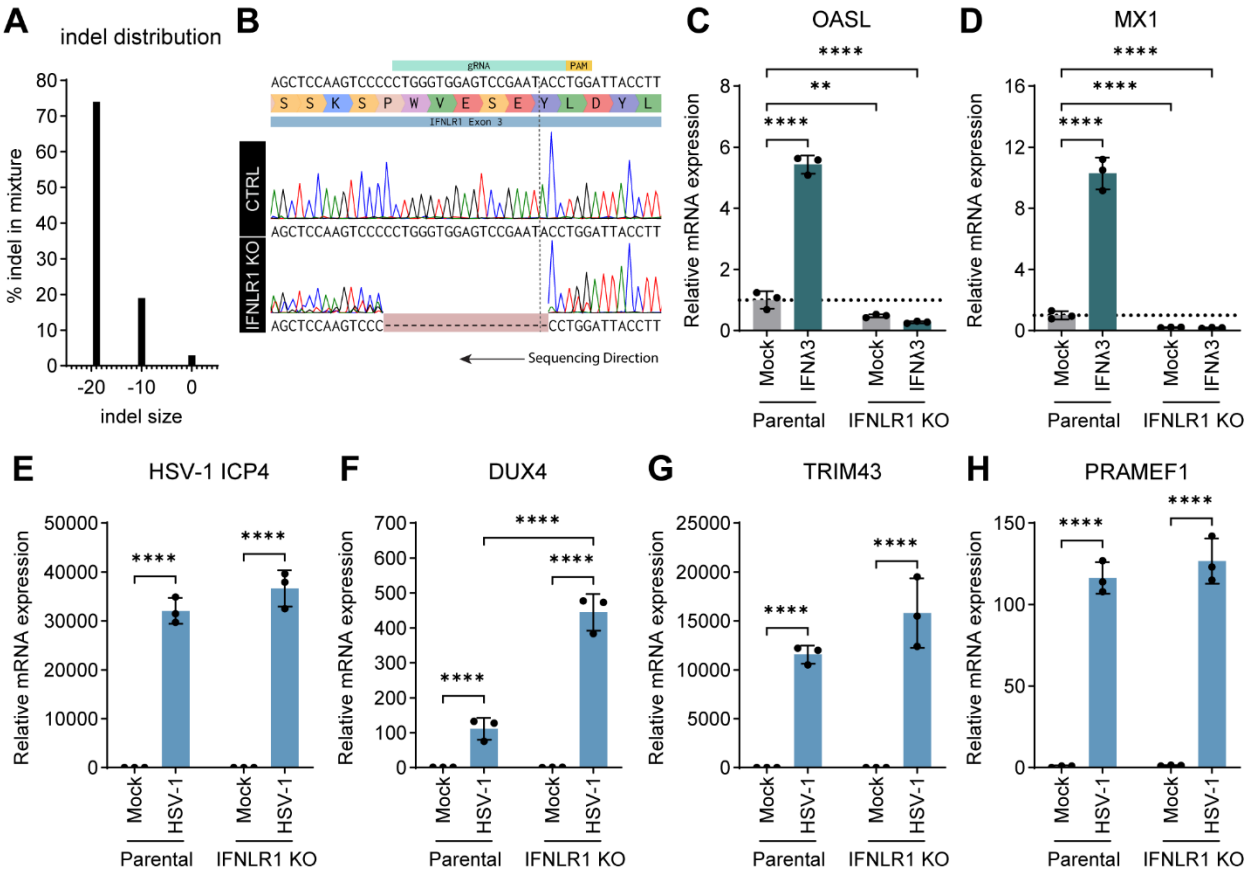

Figure 4 | Expression of DUX4 and DSGs are not dependent on constitutive type-III IFN signaling. TOs were transduced with lentiviral vectors engineered to express Cas9 and an sgRNA to target exon three of the human IFNLR1 locus. Single cell cloning was used to isolate homogenous organoid lines. PCR amplicons of the sgRNA target site were sent for sanger sequencing and analyzed using the Synthego ICE tool. **(A)** Predicted indel distribution of the IFNLR1 KO clone. **(B)** Sanger sequencing traces of the IFNLR1 KO clone aligned to a control sequencing trace. Sequencing proceeded from right to left as the traces are displayed. **(C-D)** IFNLR1 KO and parental organoids grown on matrigel coats were mock-treated or treated with 5 ng/µL IFNλ3. qRT-PCR was used to measure the expression of the ISGs *OASL* and *MX1*. **(E-H)** IFNLR1 KO and parental organoids grown on matrigel coats were infected with HSV-1 to induce DUX4/DSGs. qRT-PCR was used to measure the expression of HSV-1 ICP4, *DUX4*, *TRIM43B*, and *PRAMEF1*. Values are plotted as expression relative to parental mock and each individual data point is displayed. Bars display mean ± SD. Statistical significance was determined by ANOVA with the Tukey multiple comparisons tests. * $p < 0.05$, ** $p < 0.01$, **** $p < 0.0001$.

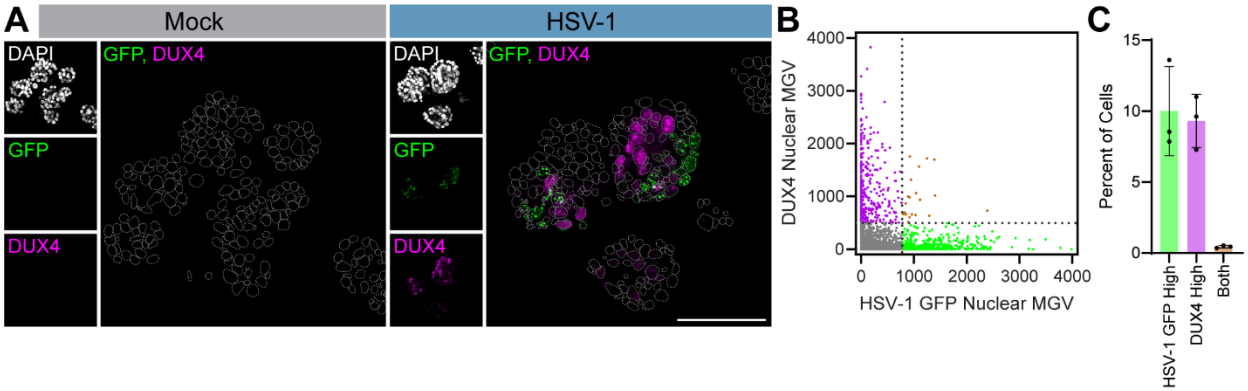

Figure 5 | DUX4 expression inversely correlates with HSV-1 gene expression in trophoblast organoids. TOs were grown on coats and infected with HSV-1 (MOI of 5). DUX4 was stained by immunofluorescence and DUX4 and HSV-1 GFP-UL25 were imaged by confocal microscopy. **(A)** Confocal micrographs of mock-infected and HSV-1-infected trophoblast organoids. Individual channels are displayed to the left with DAPI in gray, GFP-UL25 in green, and DUX4 in magenta. Nuclear outlines are shown in the merged image as dashed gray lines. Scale bar = 100 µm. **(B)** Quantification of nuclear mean gray value (MGV) of DUX4 and HSV-1 GFP-UL25. Each dot represents an individual nucleus. **(C)** Bar graph of the proportion of cells determined HSV-1 GFP-high, DUX4-high, or both. Black circles represent each independent datapoint. Bars display mean ± SD.

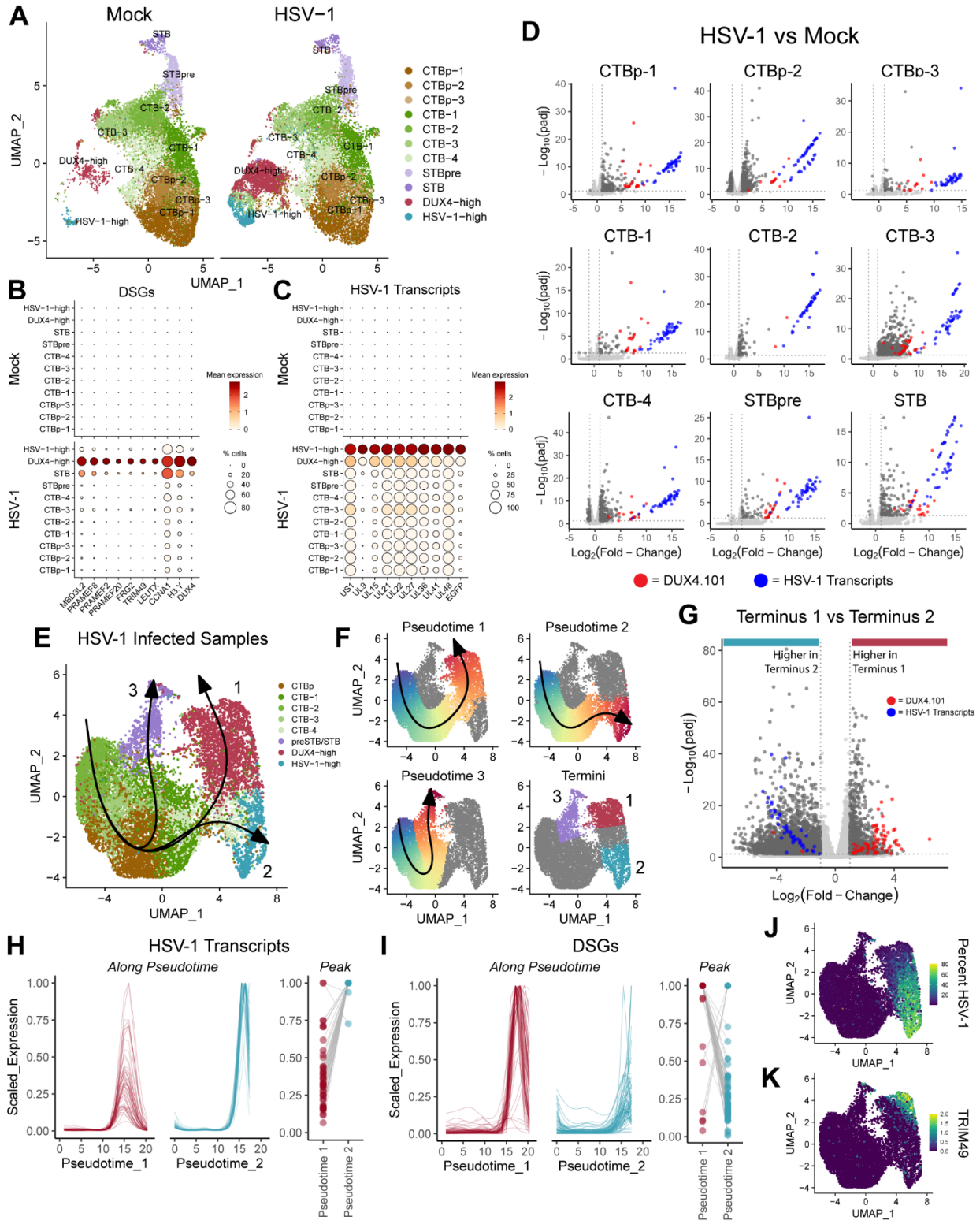

Figure 6 | DUX4-stimulated genes define a low viral gene expression trajectory in HSV-1-infected trophoblast organoids. TOs released from matrigel were infected with HSV-1 in suspension then returned to matrigel imbedding. HSV-1-infected and mock-infected organoids from two donors (2x TO74 samples and 1x TO84 sample each) were analyzed by scRNAseq. **(A)**

UMAP of clusters from all mock-infected and all HSV-1-infected TOs separated by infection status. Clusters are labeled as proliferative cytotrophoblasts (CTBp), cytotrophoblasts (CTB), pre-syncytiotrophoblasts (STBpre), syncytiotrophoblasts (STB), DUX4-high cells, or HSV-1-high cells. Multiple clusters from a single cell type are annotate with a -number after the cluster name. **(B-C)** Dot plots showing the average expression (ALRA assay) and proportion of cells expressing selected DSGs (B) and HSV-1 transcripts (C) in each cluster separated into mock-infected samples (top) and HSV-1-infected samples (bottom). **(D)** Pseudobulk analysis identifying significant DEGs (Log2(fold-change) > 1 and adjusted *p*-value < 0.05) between HSV-1-infected samples and mock-infected samples. Results from all clusters other than the DUX4-high and HSV-1-high clusters are shown. Genes that belong to the DUX4.101 list are displayed as red circles and HSV-1 transcripts are displayed as blue circles. Also see **Table S6**. **(E)** UMAP of re-clustered cells from HSV-1 infected samples with >0.1% HSV-1 reads. Clusters are labeled as CTBp, CTB, preSTB/STB, DUX4-high, or HSV-1-high. Multiple clusters from a single cell type are annotate with a -number after the cluster name. Slingshot trajectories are superimposed and numbered. **(F)** Featureplots of the pseudotime values (0-100) assigned to each cell along each trajectory (top and lower left). Featureplot showing the cells that were part of the final 15% of cells in a trajectory and designated as part of a trajectory terminus (lower right). **(G)** Pseudobulk analysis identifying significant DEGs (Log2(fold-change) > 1 and adjusted *p*-value < 0.05) between terminus 1 and terminus 2. Genes that belong to the DUX4.101 list are displayed as red circles and HSV-1 transcripts are displayed as blue circles. **(H-I)** Plots of the average expression (scaled to between 0 and 1) of all HSV-1 transcripts (H) and all DSGs (I) along pseudotime 1 and pseudotime 2. Relative peak expression of each HSV-1 transcript (H) and each DSG (I) along each trajectory is shown in a plot to the right. **(J-K)** Featureplots showing percent HSV-1 reads (J) and the expression of the DSG *TRIM49* (K).

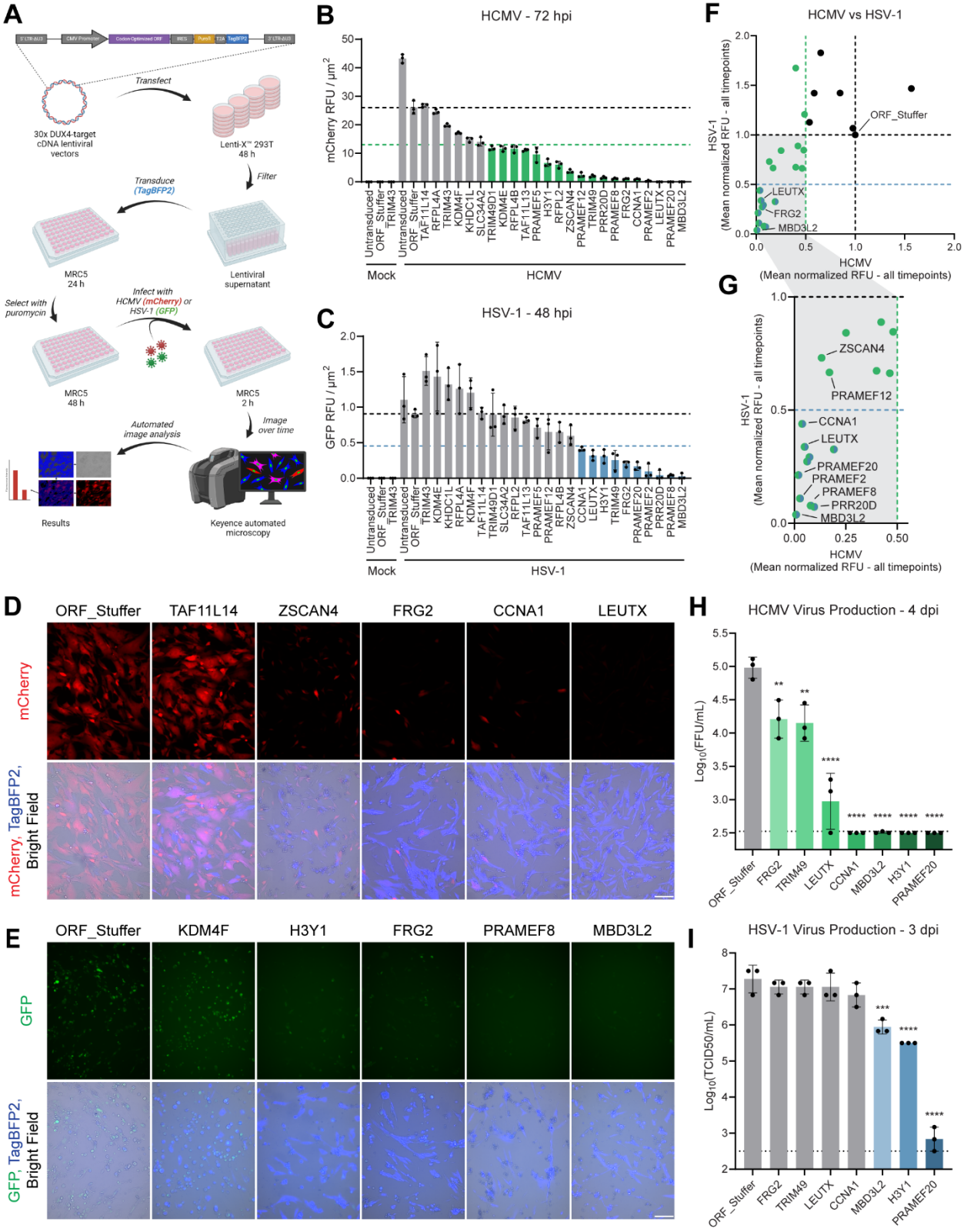
A
5' LTR-Δ U3
CMV Promoter
Codon-Optimized ORF
IRES
PuroR
T2A
TagBFP2
3' LTR-Δ U3
Transfect
30x DUX4-target cDNA lentiviral vectors
Lenti-X™ 293T 48 h
Filter
Transduce (TagBFP2)
MRC5 24 h
Lentiviral supernatant
Select with puromycin
Infect with HCMV (mCherry) or HSV-1 (GFP)
MRC5 48 h
MRC5 2 h
Image over time
Automated image analysis
Results
Keyence automated microscopy
B
HCMV - 72 hpi
mCherry RFU / µm²
Untransduced
ORF_Stuffer
TRIM43
TAF11L14
RFPL4A
KDM4F
KHDC1L
SLC34A2
TRIM49D1
KDM4E
RFPL4B
TAF11L13
PRAMEF5
H3Y1
RFPL2
ZSCAN4
PRAMEF12
TRIM49
PRR20D
PRAMEF8
FRG2
CCNA1
PRAMEF2
LEUTX
PRAMEF20
MBD3L2
Mock
HCMV
C
HSV-1 - 48 hpi
GFP RFU / µm²
HSV-1
F
HCMV vs HSV-1
HSV-1 (Mean normalized RFU - all timepoints)
HCMV (Mean normalized RFU - all timepoints)
ORF_Stuffer
LEUTX
FRG2
MBD3L2
G
ZSCAN4
PRAMEF12
CCNA1
LEUTX
PRAMEF20
PRAMEF2
PRAMEF8
PRR20D
MBD3L2
D
ORF_Stuffer
TAF11L14
ZSCAN4
FRG2
CCNA1
LEUTX
mCherry
mCherry, TagBFP2, Bright Field
H
HCMV Virus Production - 4 dpi
Log10(FFU/mL)
ORF_Stuffer
FRG2
TRIM49
LEUTX
CCNA1
MBD3L2
H3Y1
PRAMEF20
E
ORF_Stuffer
KDM4F
H3Y1
FRG2
PRAMEF8
MBD3L2
GFP
GFP, TagBFP2, Bright Field
I
HSV-1 Virus Production - 3 dpi
Log10(TCID50/mL)
ORF_Stuffer
FRG2
TRIM49
LEUTX
CCNA1
MBD3L2
H3Y1
PRAMEF20

973

Figure 7 | DUX4-stimulated genes exert anti-herpesvirus activity, (A) Schematic representing the screening method in MRC5 cells. **(B-C)** Bar graphs depicting representative timepoints for HCMV (B; 72 hpi) and HSV-1 (C; 48 hpi). Black circles represent each individual datapoint. Bars display mean ± SD. **(D)** Representative DSGs for HCMV: one with minimal impact and four top hits. Widefield micrographs of representative fields from 72 hpi. mCherry is portrayed in red in the top row, and merged mCherry (red), TagBFP2 (blue), and brightfield (grayscale) is portrayed in the bottom row. Scale bars = 200 µm. **(E)** Representative DSGs for HSV-1: one with minimal impact and four top hits. Widefield micrographs of representative fields from 48 hpi. GFP is portrayed in green in the top row, and merged GFP (green), TagBFP2 (blue), and brightfield (grayscale) is portrayed in the bottom row. Scale bars = 200 µm. **(F)** Mean normalized relative fluorescence units (RFU) from HCMV in cells expressing each DSG plotted against the mean normalized RFU from HSV-1 in cells expressing each DSG (mean of all timepoints). **(G)** Zoomed in view of panel (F). Black dashed lines in graphs B, C, F, and G represent the mean expression of ORF_Stuffer. Colored dashed lines represent 0.5x the black line. (H-I) Bar graphs depicting virus production from HCMV (H) and HSV-1 (I). HCMV and HSV-1 infectious particles were quantified as focus-forming units (FFU) and 50% tissue culture infectious dose (TCID50) respectively. Black circles represent each individual datapoint. Bars display mean ± SD.Black dotted lines in these graphs represent the limit of detection. Significance was determined by ANOVA with the Tukey multiple comparisons tests. ** $p < 0.01$, *** $p < 0.001$, **** $p < 0.0001$.

994 **Extended Data Figures and Legends**

995

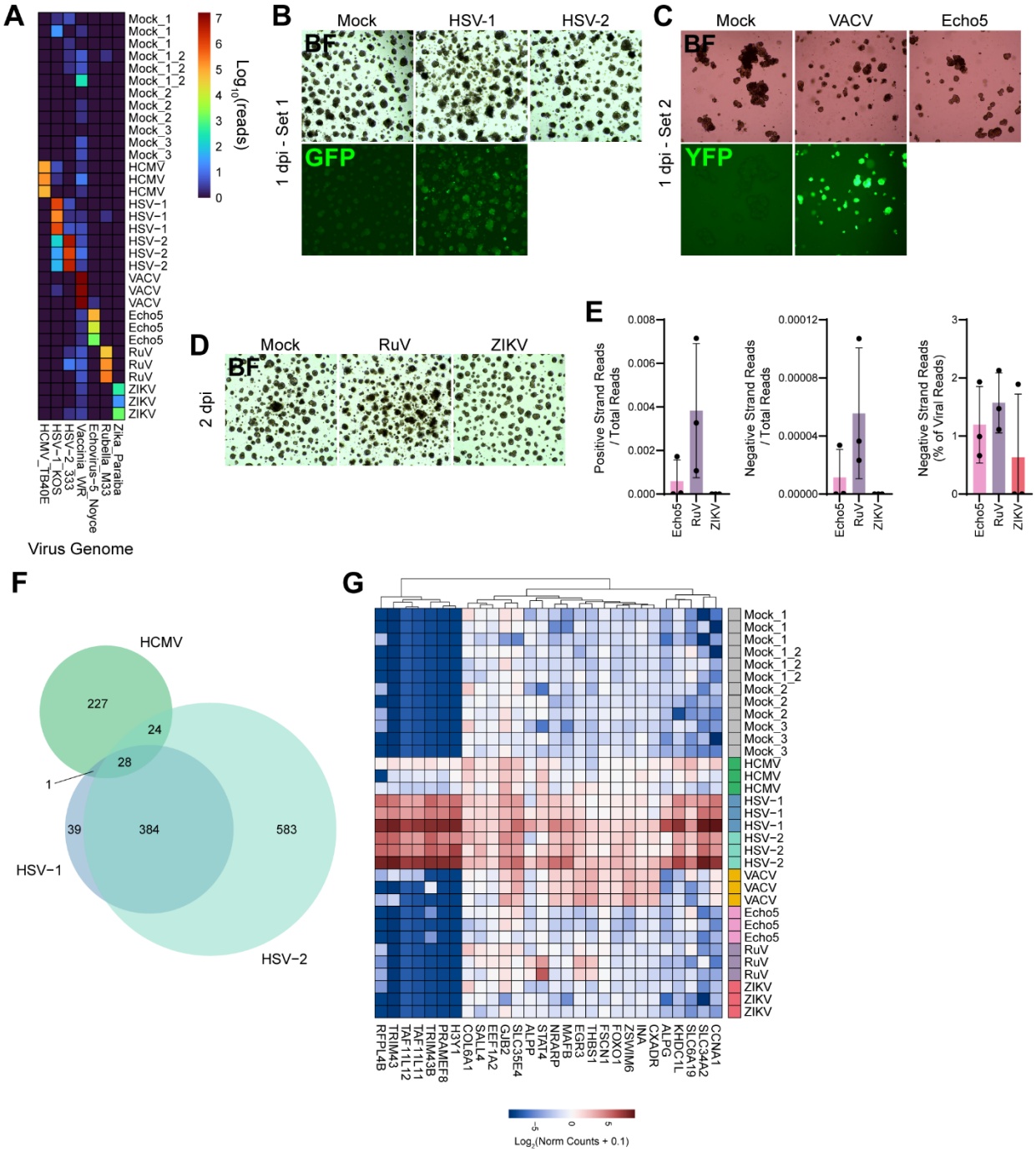

996

997 **Figure S1 | Trophoblast organoids respond distinctly to diverse viruses.** Trophoblast
998 organoids from three donors were infected with HCMV, HSV-1, HSV-2, VACV, Echo5, RuV, and
999 ZIKV at an MOI of 2. VACV and Echo5 infections were performed in suspension on organoids
1000 released from matrigel that were re-imbedded in matrigel following inoculation. All other infections
1001 were performed on spherical organoids grown on matrigel coats. mRNA was purified and
1002 analyzed by RNAseq. **(A)** Heatmap portraying the $\log_{10}$ reads that map to each of the viral
1003 genomes. **(B-D)** Microscopic images of mock and infected organoids. Bright field (BF) images are
1004 in the first row of each panel. Fluorescence images were included for HSV-1 (B) and VACV (C).

1005 **(D)** Bar plots of the number of reads mapping to the positive and negative strand of the Echo5,
1006 RuV, and ZIKV genomes normalized to the total reads in the sample (left two graphs). Bar plot of
1007 the percent of viral reads that mapped to the negative strand of the viral genome (right graph).
1008 Bars display mean ± SD. Black dots represent each individual data point. **(F)** Venn diagram
1009 denoting the number of shared DEGs between each of the herpesvirus infection conditions. **(G)**
1010 Heatmap portraying the genes that are induced by all three herpesviruses in TOs. Values are $\log_2$
1011 normalized counts from DESeq2 analysis plus a pseudo count of 0.1. Key is at the bottom. Red
1012 indicates higher expression and blue indicates lower expression. Hierarchical clustering of genes
1013 is shown at the top.

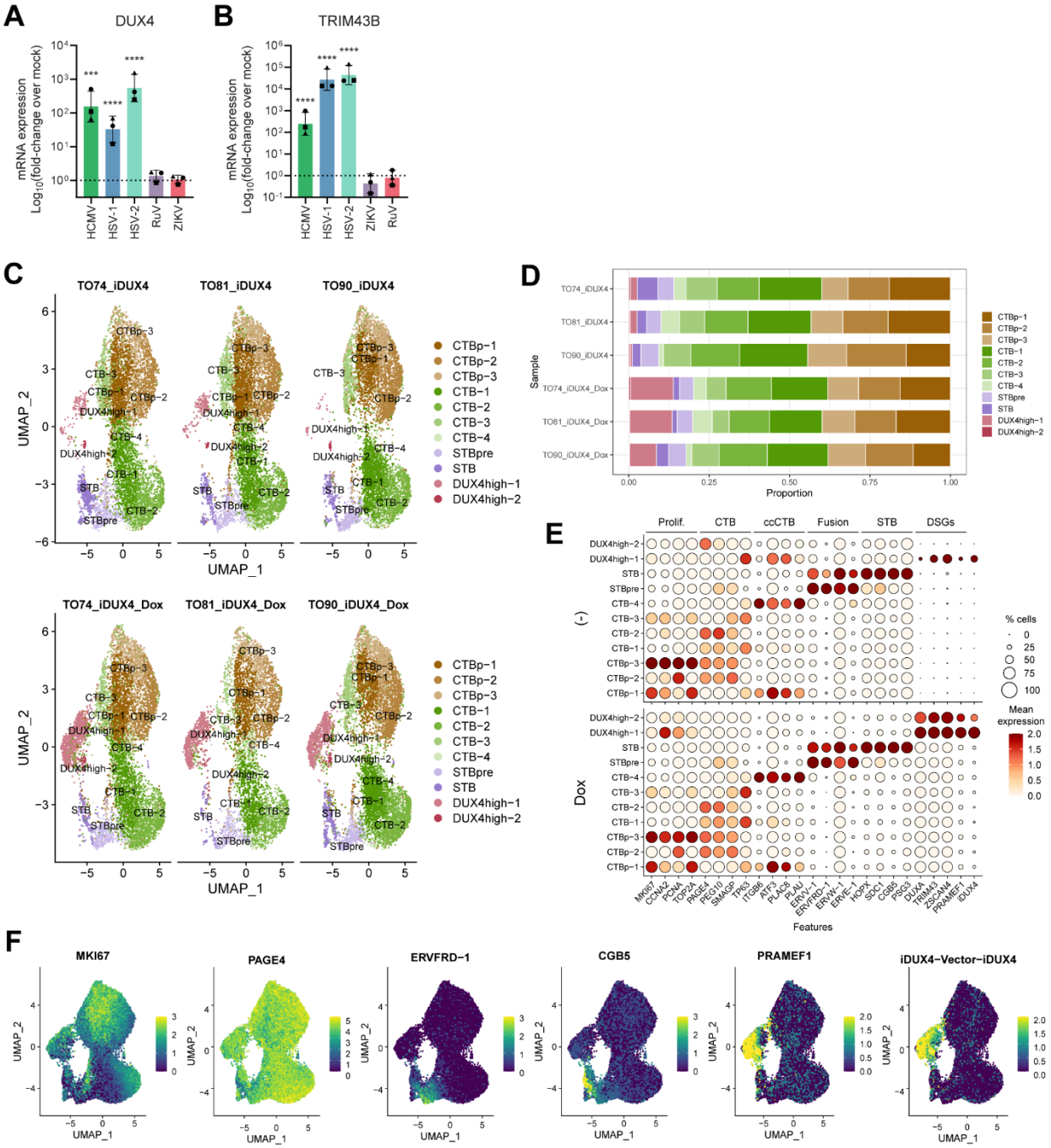

Figure S2 | Trophoblasts respond to herpesviruses with DUX4-stimulated genes. (A-B) Bar plot portraying the expression of *DUX4* and the DSG *TRIM43* as measured by qRT-PCR following the infection of TOs from three donors with HCMV, HSV-1, HSV-2, RuV, and ZIKV. Values are plotted as Log_{10}(fold-change over mock). Shapes denote the donor of each data point. Bars display mean ± SD. Statistical significance was determined by ANOVA with the Tukey multiple comparisons tests. *** $p < 0.001$, **** $p < 0.0001$. **(C)** UMAP of clusters from three donors of mock-treated TOs and three donors of Dox-treated TOs separated by sample. Clusters are labeled as proliferative cytotrophoblasts (CTBp), cytotrophoblasts (CTB), pre-syncytiotrophoblasts (STBpre), syncytiotrophoblasts (STB), or DUX4-high cells. Multiple clusters from a single cell type are annotate with a -number after the cluster name. **(D)** Comparison of the

1025 proportion of cells that belong to each cluster by sample. **(E)** Dot plots showing the average
1026 expression (ALRA assay) and proportion of cells expressing selected genes in each cluster
1027 separated into mock-treated samples (top) and Dox-treated samples (bottom). The selected
1028 genes are established markers of proliferation, CTBs, cell column CTBs (ccCTBs), fusion, the
1029 STB, and DSGs. **(F)** Feature plots of representative markers of each cell type.
1030

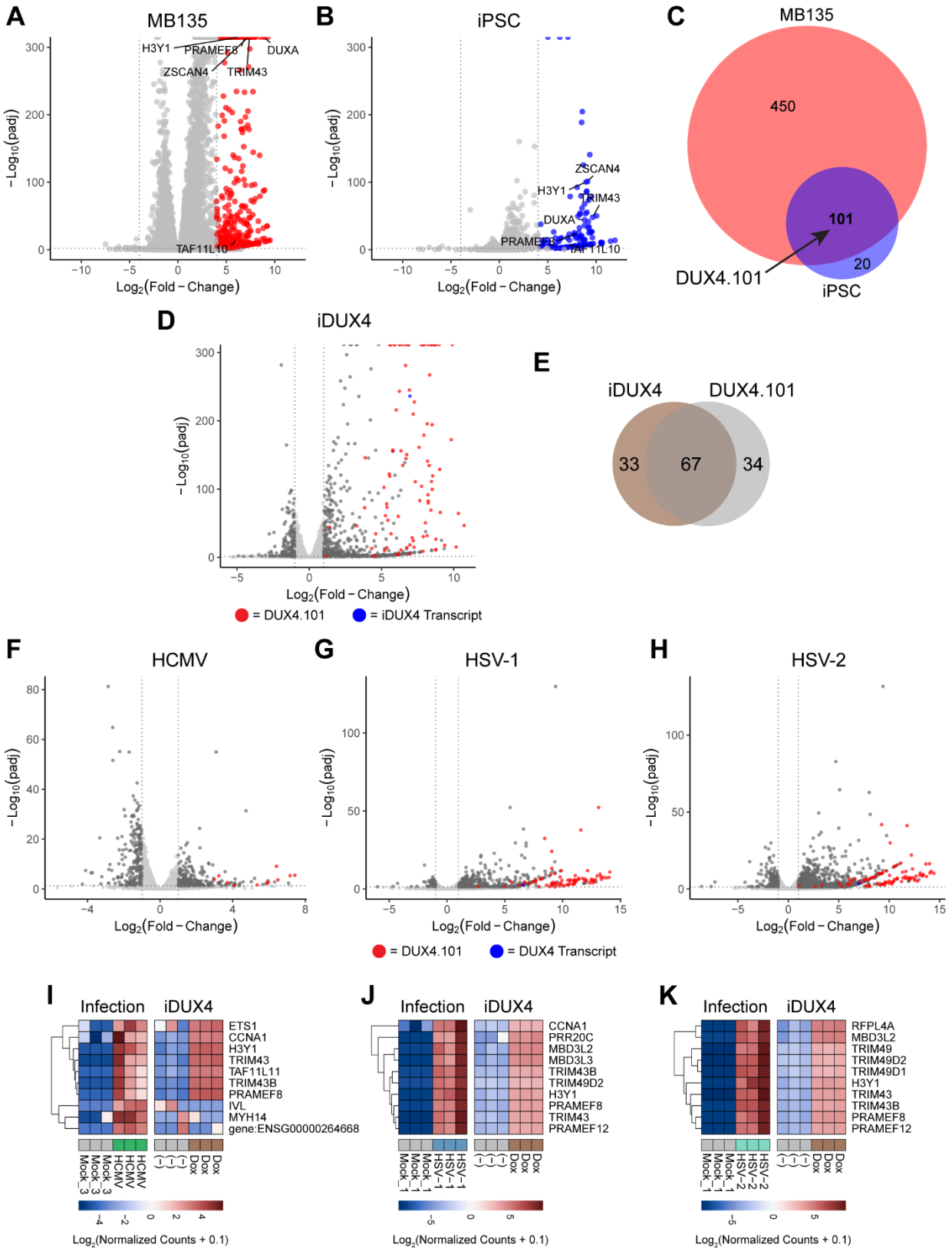

Figure S3 | Trophoblasts respond to herpesviruses with DUX4-stimulated genes. (A-B) Volcano plots portraying the DEGs upon DUX4 expression in (A) MB135 cells or (B) iPSCs. Colored circles represent significant DEGs (Log2(fold-change) > 4 and adjusted *p*-value < 0.01).

Gray circles represent genes whose expression did not meet these criteria. Also see **Table S3**. **(C)** Venn diagram denoting the overlap between the genes induced by DUX4 expression in MB135 cells and iPSCs. These 101 genes constitute the DUX4.101 list used throughout the paper as canonical DSGs that are expressed in divergent cell types. **(D)** TOs engineered to express DUX4 under a doxycycline (Dox) inducible promoter. RNAseq was performed on mock-treated and Dox-treated samples. Volcano plot portrays the DEGs upon DUX4 expression in TOs. Genes that belong to the DUX4.101 list are displayed as red circles and iDUX4 transcript is displayed as a blue circle. Significant DEGs (Log2(fold-change) > 1 and adjusted *p*-value < 0.05) are depicted in dark gray. Light gray was used to depict genes that did not meet these criteria. Also see **Table S3**. **(E)** Venn diagram denoting the overlap between the top 100 DEGs upregulated by iDUX4 expression in TOs and the DUX4.101 list of DSGs. **(F-H)** Volcano plots portraying the DEGs upon HCMV (F), HSV-1 (G), or HSV-2 (H) infection in TOs from Figure 1. Genes that belong to the DUX4.101 list are displayed as red circles and *DUX4* transcript is displayed as a blue circle. Significant DEGs (Log2(fold-change) > 1 and adjusted p-value < 0.05) are depicted in dark gray. Light gray was used to depict genes that did not meet these criteria. **(I-K)** Heatmaps comparing the expression of the top 10 genes induced by HCMV (I), HSV-1 (J), or HSV-2 (K) infection in TOs to the expression of those same genes following iDUX4 expression in TOs. Values are $\log_2$ normalized counts from DESeq2 analysis plus a pseudo count of 0.1. Keys are at the bottom of each chart. The scale is not constant between each heatmap. Red indicates higher expression and blue indicates lower expression. Hierarchical clustering of genes is shown to the left.

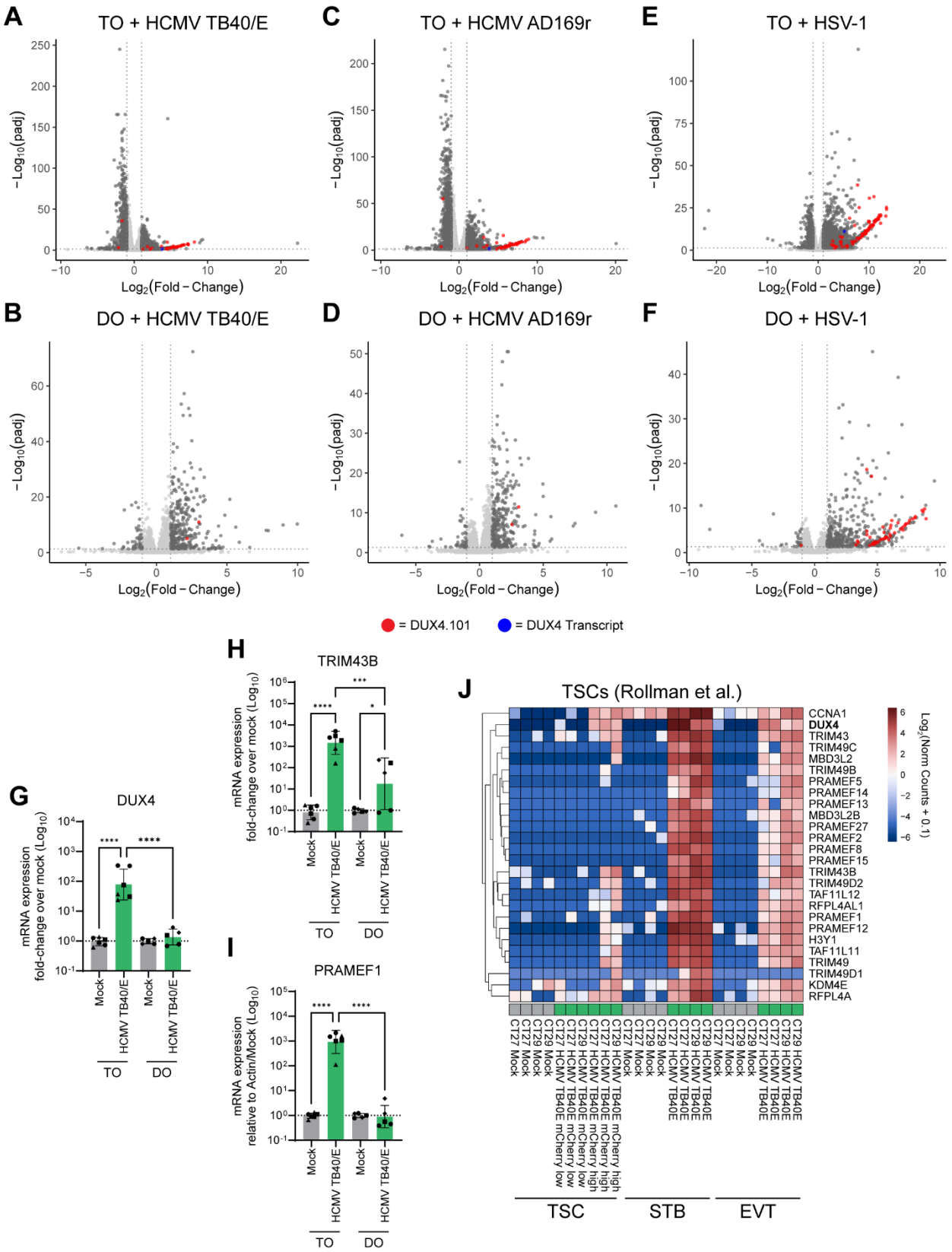

Figure S4 | DUX4-stimulated genes are induced to higher levels in trophoblasts than maternal decidual epithelial cells. RNAseq analysis was employed to assess if TOs and DOs

differentially express DUX4 or DSGs when infected with HCMV TB40/E, HCMV AD169r, and HSV-1. Also see **Table S5**. **(A-F)** Volcano plots portraying the DEGs upon HCMV TB40/E (A-B), HCMV AD169r (C-D), or HSV-1 (E-F) infection in TOs (top) and DOs (bottom). Genes that belong to the DUX4.101 list are displayed as red circles and DUX4 transcript is displayed as a blue circle. Significant DEGs (Log2(fold-change) > 1 and adjusted p-value < 0.05) are depicted in dark gray. Light gray was used to depict genes that did not meet these criteria. **(G-I)** TOs and DOs from three donors each (two matched and one unique to each) were infected with HCMV TB40/E and qRT-PCR was used to measure the expression of *DUX4* and the DSGs *TRIM43B* and *PRAMEF1*. Values are plotted as Log_{10}(fold-change over mock). Shapes denote the donor of each data point. Bars display mean ± SD. Statistical significance was determined by ANOVA with the Tukey multiple comparisons tests. **(J)** RNAseq analysis of mock- and HCMV-infected undifferentiated trophoblast stem cells (TSC), STB-differentiated TSCs, and EVT-differentiated TSCs. Heatmaps portraying the expression of DUX4 and canonical DSGs. Values are log_2 normalized counts from DESeq2 analysis plus a pseudo count of 0.1. Keys are at the bottom of each chart. Red indicates higher expression and blue indicates lower expression. Hierarchical clustering of genes is shown on the left. * $p < 0.05$, *** $p < 0.001$, **** $p < 0.0001$.

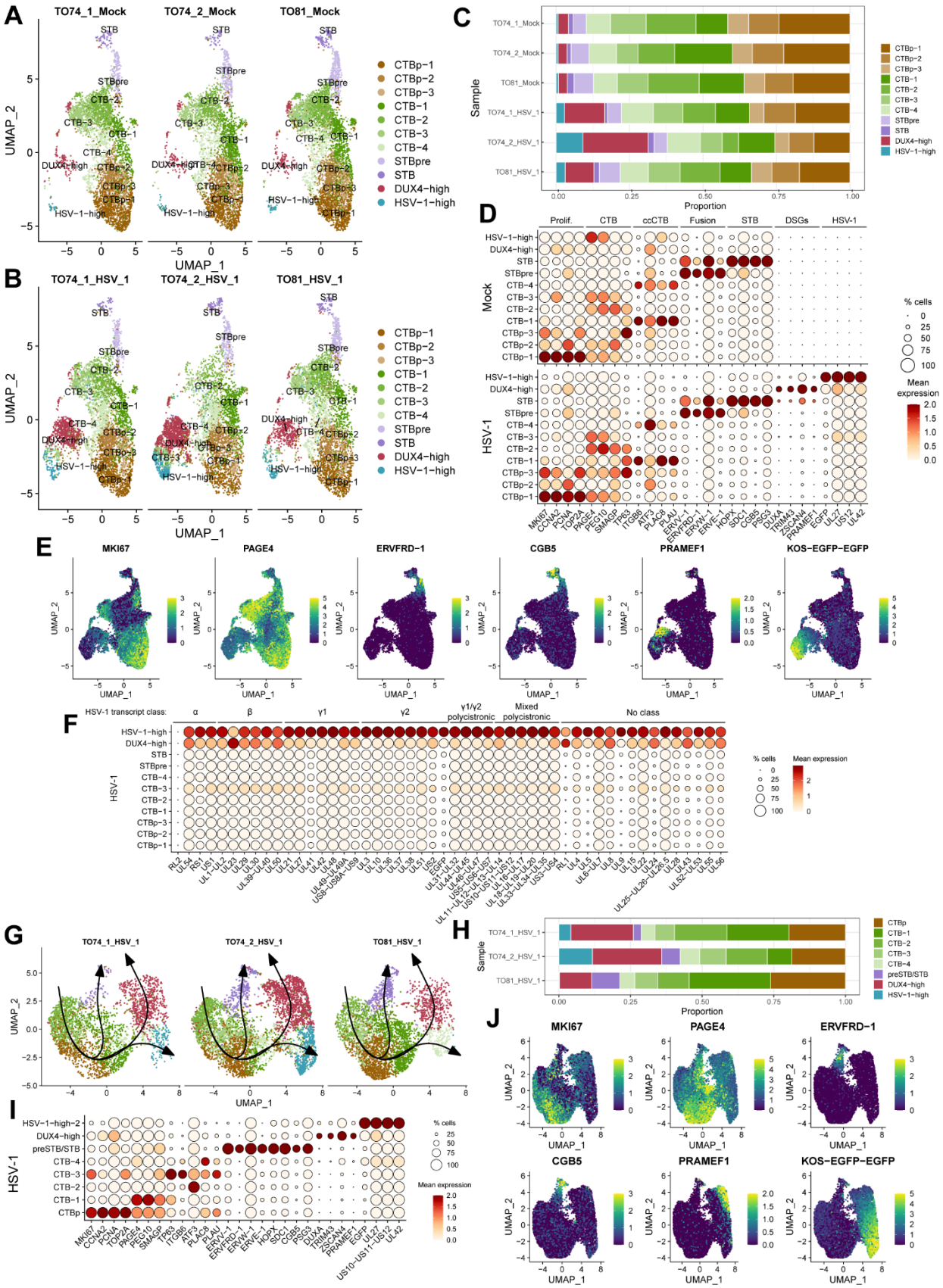
A
TO74_1_Mock
TO74_2_Mock
TO81_Mock
UMAP_1
UMAP_2
CTBp−1
CTBp−2
CTBp−3
CTB−1
CTB−2
CTB−3
CTB−4
STBpre
STB
DUX4−high
HSV−1−high
B
TO74_1_HSV_1
TO74_2_HSV_1
TO81_HSV_1
C
Sample
Proportion
D
Prolif.
CTB
ccCTB
Fusion
STB
DSGs
HSV−1
Mock
% cells
Mean expression
E
MKI67
PAGE4
ERVFRD−1
CGB5
PRAMEF1
KOS−EGFP−EGFP
F
HSV−1 transcript class:
α
β
γ1
γ2
γ1/γ2 polycistronic
Mixed polycistronic
No class
G
H
preSTB/STB
I
J

1076

Figure S5 | DUX4-stimulated genes define a low viral gene expression trajectory in HSV-1-infected trophoblast organoids. TOs released from matrigel were infected with HSV-1 in suspension then returned to matrigel imbedding. HSV-1-infected and mock-infected organoids from two donors (2x TO74 samples and 1x TO84 sample each) were analyzed by scRNAseq. **(A-B)** UMAP of clusters from all mock-infected (A) and all HSV-1-infected (B) TOs separated by sample. Clusters are labeled as proliferative cytotrophoblasts (CTBp), cytotrophoblasts (CTB), pre-syncytiotrophoblasts (STBpre), syncytiotrophoblasts (STB), DUX4-high cells, or HSV-1-high cells. Multiple clusters from a single cell type are annotate with a -number after the cluster name. **(C)** Comparison of the proportion of cells that belong to each cluster by sample. **(D)** Dot plots showing the average expression (ALRA assay) and proportion of cells expressing selected genes in each cluster separated into mock-infected samples (top) and HSV-1-infected samples (bottom). The selected genes are established markers of proliferation, CTBs, cell column CTBs (ccCTBs), fusion, the STB, DSGs, and HSV-1 transcripts. **(E)** Feature plots of representative markers of each cell type. **(F)** Dot plots showing the average expression (ALRA assay) and proportion of cells expressing all HSV-1 transcripts in each cluster. HSV-1 transcripts are organized into α (immediate early), β (early), γ1 (leaky late), γ2 (true late), γ1/γ2 polycistronic/alternatively spliced, mixed polycistronic/alternatively, and no class. **(G)** UMAP of re-clustered cells from HSV-1 infected samples with >0.1% HSV-1 reads separated by sample. Clusters are labeled as CTBp, CTB, preSTB/STB, DUX4-high, or HSV-1-high. Multiple clusters from a single cell type are annotate with a -number after the cluster name. Slingshot trajectories are superimposed. **(H)** Comparison of the proportion of cells that belong to each cluster by sample. **(I)** Dot plots showing the average expression (ALRA assay) and proportion of cells expressing selected genes in each cluster. The selected genes are established markers of proliferation, CTBs, cell column CTBs (ccCTBs), fusion, the STB, DSGs, and HSV-1 transcripts. **(J)** Feature plots of representative markers of each cell type.

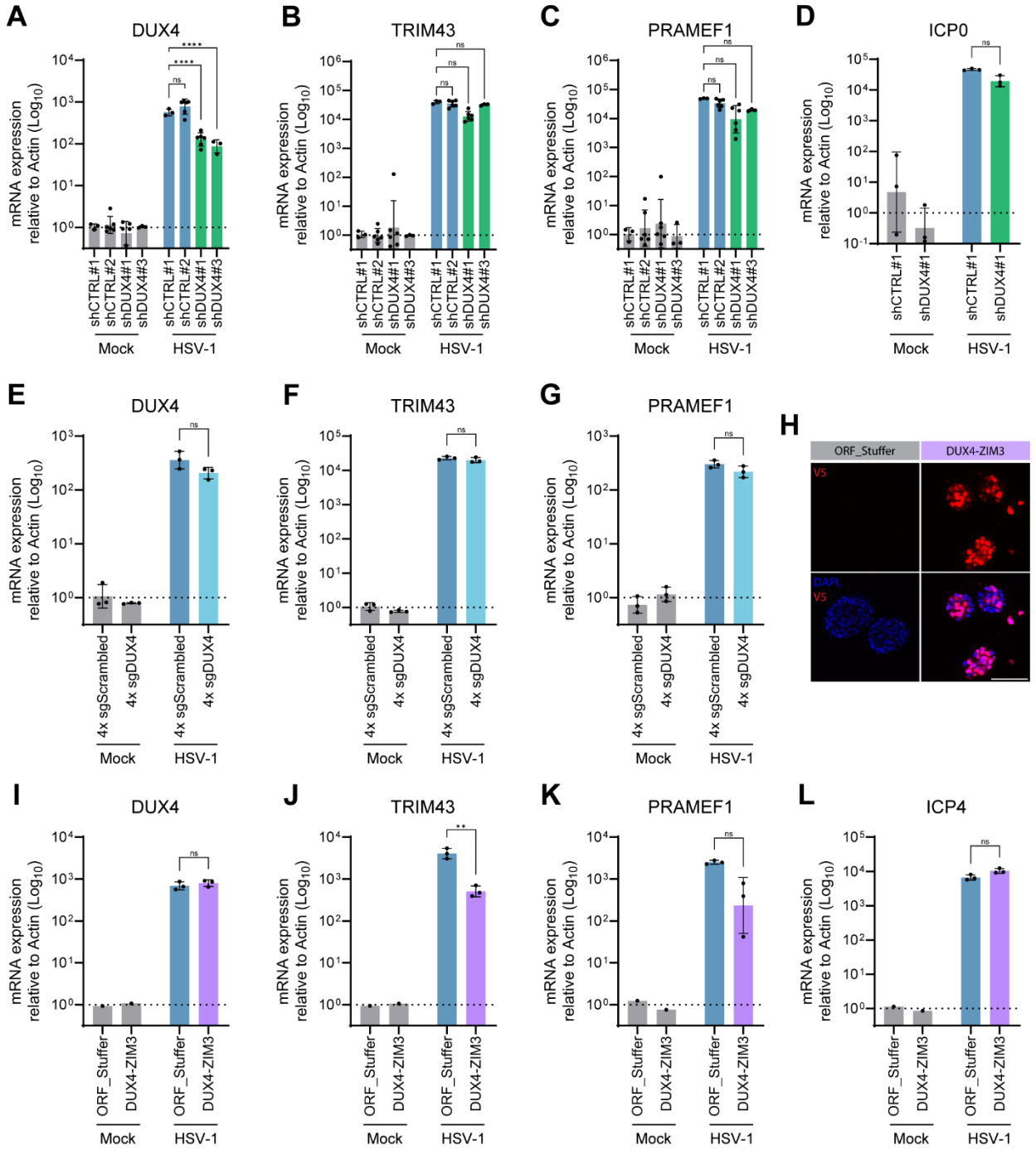

Figure S6 | DUX4 knockdown strategies in TOs. (A-D) TOs were engineered to express control (shCTRL) or *DUX4*-targeting (shDUX4) shRNAs. Engineered TOs grown on matrigel coats were infected with HSV-1 at an MOI of 5, and RNA was collected at 24 hpi. qRT-PCR was used to measure the expression of *DUX4* (A), *TRIM43* (B), *PRAMEF1* (C), and HSV-1 ICP4 (D). **(E-G)** TOs were engineered to expresses dCas9-KRAB-MeCP2 (used for CRISPRi) along with either 4 scrambled sgRNAs (4x sgScrambled) or 4 sgRNAs targeting the transcription start site of DUX4 (4x sgDUX4). Engineered TOs grown on matrigel coats were infected with HSV-1 at an MOI of 5, and RNA was collected at 24 hpi. qRT-PCR was used to measure the expression of *DUX4* (E), *TRIM43* (F), and *PRAMEF1* (G). **(H-L)** TOs were engineered to express a control vector

1113 (ORF_Stuffer) or a dominant-negative DUX4 construct with the transcriptional activation domain
1114 of DUX4 replaced with the KRAB domain of ZIM3 along with a V5 tag (DUX4-ZIM3). Confocal
1115 micrographs. V5 staining is in red and DAPI-stained nuclei are in blue. Scale bar = 100 μm (H).
1116 Engineered TOs grown on matrigel coats were infected with HSV-1 at an MOI of 5, and RNA was
1117 collected at 24 hpi. qRT-PCR was used to measure the expression of *DUX4* (I), *TRIM43* (J),
1118 *PRAMEF1* (K), and HSV-1 ICP0 (L).
1119

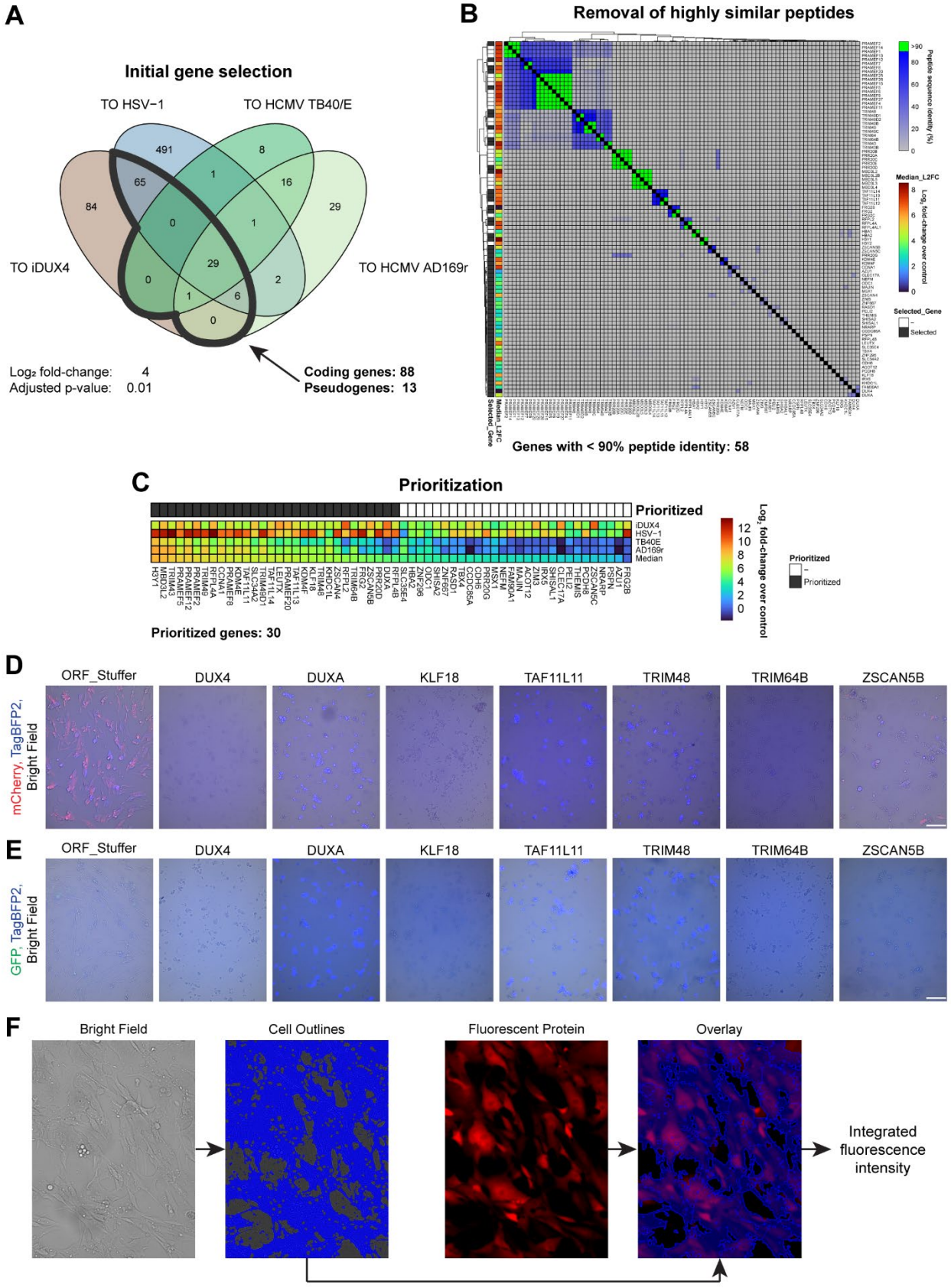
A
Initial gene selection
TO HSV−1
TO HCMV TB40/E
TO iDUX4
TO HCMV AD169r
491
8
65
1
16
84
29
0
1
29
0
2
1
6
0
Log₂ fold-change: 4
Adjusted p-value: 0.01
Coding genes: 88
Pseudogenes: 13
B
Removal of highly similar peptides
Peptide sequence identity (%)
Median_L2FC
Log₂ fold-change over control
Selected_Gene
Selected
Genes with < 90% peptide identity: 58
C
Prioritization
Prioritized
iDUX4
HSV−1
TB40E
AD169r
Median
Log₂ fold-change over control
Prioritized genes: 30
D
ORF_Stuffer
DUX4
DUXA
KLF18
TAF11L11
TRIM48
TRIM64B
ZSCAN5B
mCherry, TagBFP2, Bright Field
E
GFP, TagBFP2, Bright Field
F
Bright Field
Cell Outlines
Fluorescent Protein
Overlay
Integrated fluorescence intensity

1120

1121 **Figure S7 | DUX4-stimulated genes exert anti-herpesvirus activity. (A)** Venn diagram
1122 depicting the overlap between DEGs induced by iDUX4 expression or HSV-1, HCMV TB40/E, or
1123 HCMV AD169r infection in TOs (Log_2(fold-change) > 4 and adjusted p-value < 0.01). Thick line
1124 highlights the selected genes. **(B)** Heatmap depicting the percent peptide sequence identity
1125 between genes selected in (A). Genes with >90% peptide sequence identity are highlighted in
1126 green. Median log_2 fold-change over control from iDUX4 expression and HSV-1, HCMV TB40/E,
1127 and HCMV AD169r infection in TOs are displayed to the left. Genes selected for further
1128 consideration are marked in gray to the left. **(C)** Heatmap depicting the log_2 fold-change over
1129 control from iDUX4 expression and HSV-1, HCMV TB40/E, and HCMV AD169r infection in TOs.
1130 Genes are ordered by median log_2 fold-change over control. Prioritized genes are marked in gray
1131 to the top. **(D-E)** DUX4 and six DSGs were toxic to MRC5 cells. Widefield micrographs of
1132 representative fields from HCMV (D) and HSV-1 (E) infection at 24 hpi. Images portray merged
1133 TagBFP2 (blue), brightfield (grayscale), and mCherry (D; red; HCMV) or GFP (E; green; HSV-1).
1134 **(F)** Schematic of image quantification method. Scale bars = 200 μm.
1135

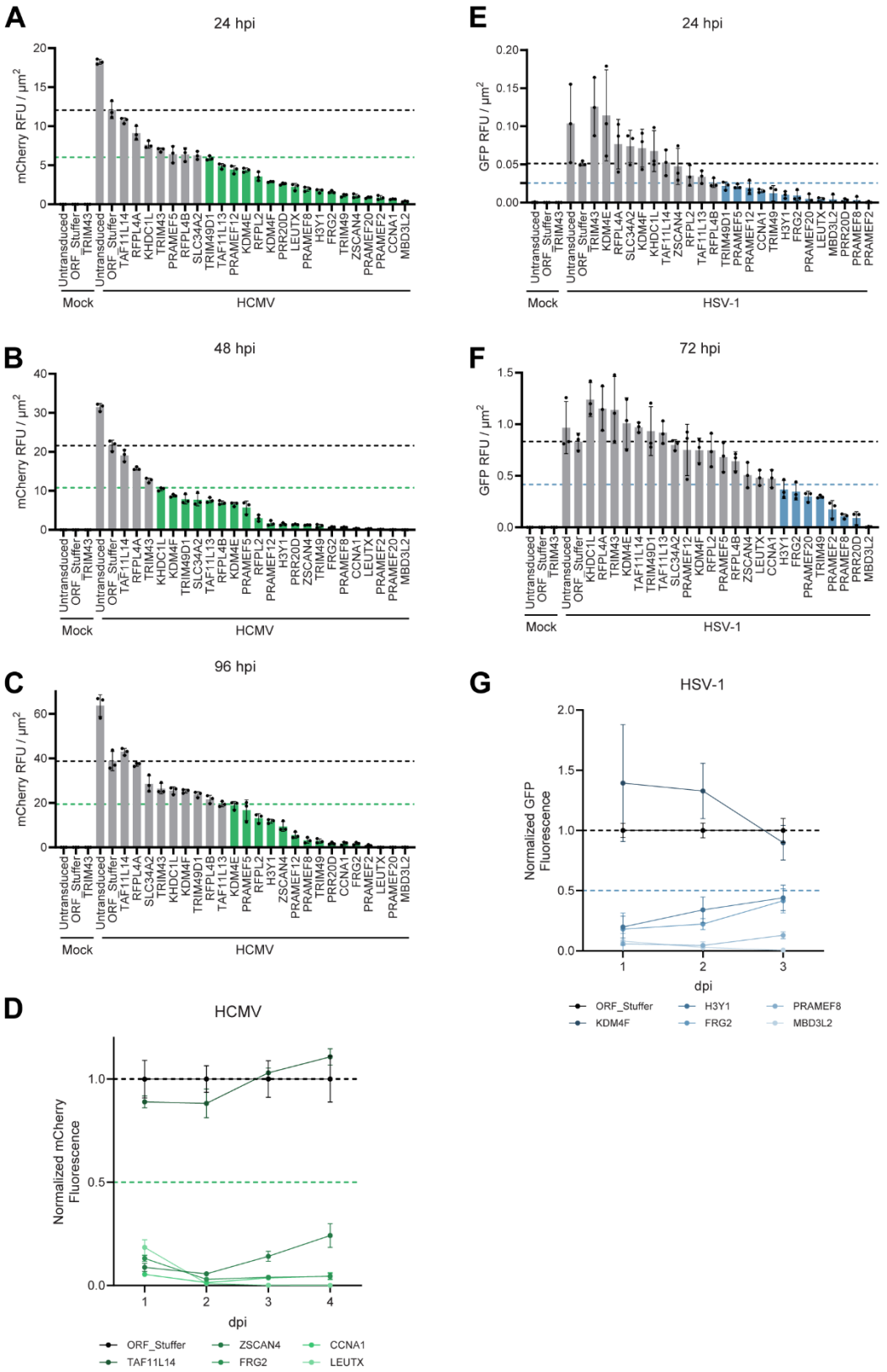

Figure S8 | DUX4-stimulated genes exert anti-herpesvirus activity. (A-C and E-F) Bar graphs depicting timepoints for HCMV (A-C) and HSV-1 (E-F) not shown in Figure 7. Black circles

represent each individual datapoint. Bars display mean ± SD. **(D and G)** Representative DSGs for HCMV: one with minimal impact and four top hits. Normalized mCherry fluorescence from HCMV for these genes at all timepoints (D). Representative DSGs for HSV-1: one with minimal impact and four top hits. Normalized GFP fluorescence from HSV-1 for these genes at all timepoints (G). Dots and error bars display mean ± SD. Black dashed lines in graphs represent the mean expression of ORF_Stuffer. Colored dashed lines represent 0.5x the black line.

1146 ## References

1147 1. Ander, S.E., Diamond, M.S., and Coyne, C.B. (2019). Immune responses at the maternal-
1148 fetal interface. Sci Immunol *4*. 10.1126/sciimmunol.aat6114.

1149 2. Megli, C.J., and Coyne, C.B. (2022). Infections at the maternal-fetal interface: an overview
1150 of pathogenesis and defence. Nat Rev Microbiol *20*, 67-82. 10.1038/s41579-021-00610-
1151 y.

1152 3. Pontes, K.F.M., Nardozza, L.M.M., Peixoto, A.B., Werner, H., Tonni, G., Granese, R., and
1153 Araujo Junior, E. (2024). Cytomegalovirus and Pregnancy: A Narrative Review. J Clin Med
1154 *13*. 10.3390/jcm13020640.

1155 4. Winter, A.K., and Moss, W.J. (2022). Rubella. Lancet *399*, 1336-1346. 10.1016/S0140-
1156 6736(21)02691-X.

1157 5. Lamont, R.F., Sobel, J.D., Carrington, D., Mazaki-Tovi, S., Kusanovic, J.P., Vaisbuch, E.,
1158 and Romero, R. (2011). Varicella-zoster virus (chickenpox) infection in pregnancy. BJOG
1159 *118*, 1155-1162. 10.1111/j.1471-0528.2011.02983.x.

1160 6. Sandoni, M., Ciardo, L., Tamburini, C., Boncompagni, A., Rossi, C., Guidotti, I., Garetti,
1161 E., Lugli, L., Iughetti, L., and Berardi, A. (2022). Enteroviral Infections in the First Three
1162 Months of Life. Pathogens *11*. 10.3390/pathogens11010060.

1163 7. Shi, T.L., Huang, L.J., Xiong, Y.Q., Zhong, Y.Y., Yang, J.J., Fu, T., Lei, X.F., and Chen,
1164 Q. (2018). The risk of herpes simplex virus and human cytomegalovirus infection during
1165 pregnancy upon adverse pregnancy outcomes: A meta-analysis. J Clin Virol *104*, 48-55.
1166 10.1016/j.jcv.2018.04.016.

1167 8. Fowler, K.B., Ross, S.A., Shimamura, M., Ahmed, A., Palmer, A.L., Michaels, M.G.,
1168 Bernstein, D.I., Sanchez, P.J., Feja, K.N., Stewart, A., and Boppana, S. (2018). Racial
1169 and Ethnic Differences in the Prevalence of Congenital Cytomegalovirus Infection. J
1170 Pediatr *200*, 196-201 e191. 10.1016/j.jpeds.2018.04.043.

1171 9. Kenneson, A., and Cannon, M.J. (2007). Review and meta-analysis of the epidemiology
1172 of congenital cytomegalovirus (CMV) infection. Rev Med Virol *17*, 253-276.
1173 10.1002/rmv.535.

1174 10. Shimada, K., Toriyabe, K., Kitamura, A., Morikawa, F., Minematsu, T., Ikejiri, M., Suga, S.,
1175 Toyoda, H., Amano, K., Kitano, M., et al. (2021). Primary cytomegalovirus infection during
1176 pregnancy and congenital infection: a population-based, mother-child, prospective cohort
1177 study. J Perinatol *41*, 2474-2481. 10.1038/s41372-021-01157-9.

1178 11. Delorme-Axford, E., Donker, R.B., Mouillet, J.F., Chu, T., Bayer, A., Ouyang, Y., Wang,
1179 T., Stolz, D.B., Sarkar, S.N., Morelli, A.E., et al. (2013). Human placental trophoblasts
1180 confer viral resistance to recipient cells. Proc Natl Acad Sci U S A *110*, 12048-12053.
1181 10.1073/pnas.1304718110.

1182 12. Bayer, A., Lennemann, N.J., Ouyang, Y., Bramley, J.C., Morosky, S., Marques, E.T., Jr.,
1183 Cherry, S., Sadovsky, Y., and Coyne, C.B. (2016). Type III Interferons Produced by

1184 Human Placental Trophoblasts Confer Protection against Zika Virus Infection. Cell Host
1185 Microbe *19*, 705-712. 10.1016/j.chom.2016.03.008.

1186 13. Pollheimer, J., Vondra, S., Baltayeva, J., Beristain, A.G., and Knofler, M. (2018).
1187 Regulation of Placental Extravillous Trophoblasts by the Maternal Uterine Environment.
1188 Front Immunol *9*, 2597. 10.3389/fimmu.2018.02597.

1189 14. Buchrieser, J., Degrelle, S.A., Couderc, T., Nevers, Q., Disson, O., Manet, C., Donahue,
1190 D.A., Porrot, F., Hillion, K.H., Perthame, E., et al. (2019). IFITM proteins inhibit placental
1191 syncytiotrophoblast formation and promote fetal demise. Science *365*, 176-180.
1192 10.1126/science.aaw7733.

1193 15. Yockey, L.J., Jurado, K.A., Arora, N., Millet, A., Rakib, T., Milano, K.M., Hastings, A.K.,
1194 Fikrig, E., Kong, Y., Horvath, T.L., et al. (2018). Type I interferons instigate fetal demise
1195 after Zika virus infection. Sci Immunol *3*. 10.1126/sciimmunol.aao1680.

1196 16. Zani, A., Zhang, L., McMichael, T.M., Kenney, A.D., Chemudupati, M., Kwiek, J.J., Liu,
1197 S.L., and Yount, J.S. (2019). Interferon-induced transmembrane proteins inhibit cell fusion
1198 mediated by trophoblast syncytins. J Biol Chem *294*, 19844-19851.
1199 10.1074/jbc.AC119.010611.

1200 17. Casazza, R.L., Lazear, H.M., and Miner, J.J. (2020). Protective and Pathogenic Effects of
1201 Interferon Signaling During Pregnancy. Viral Immunol *33*, 3-11. 10.1089/vim.2019.0076.

1202 18. Corry, J., Arora, N., Good, C.A., Sadovsky, Y., and Coyne, C.B. (2017). Organotypic
1203 models of type III interferon-mediated protection from Zika virus infections at the maternal-
1204 fetal interface. Proc Natl Acad Sci U S A *114*, 9433-9438. 10.1073/pnas.1707513114.

1205 19. Wickramage, I., VanWye, J., Max, K., Lockhart, J.H., Hortu, I., Mong, E.F., Canfield, J.,
1206 Lamabadu Warnakulasuriya Patabendige, H.M., Guzeloglu-Kayisli, O., Inoue, K., et al.
1207 (2023). SINE RNA of the imprinted miRNA clusters mediates constitutive type III interferon
1208 expression and antiviral protection in hemochorial placentas. Cell Host Microbe *31*, 1185-
1209 1199 e1110. 10.1016/j.chom.2023.05.018.

1210 20. Yang, L., Semmes, E.C., Ovies, C., Megli, C., Permar, S., Gilner, J.B., and Coyne, C.B.
1211 (2022). Innate immune signaling in trophoblast and decidua organoids defines differential
1212 antiviral defenses at the maternal-fetal interface. Elife *11*. 10.7554/eLife.79794.

1213 21. Rollman, T.B., Berkebile, Z.W., Okae, H., Bardwell, V.J., Gearhart, M.D., and Bierle, C.J.
1214 (2024). Human trophoblast stem cells restrict human cytomegalovirus replication. J Virol
1215 *98*, e0193523. 10.1128/jvi.01935-23.

1216 22. Schatten, H., and Constantinescu, G.M. (2007). Comparative reproductive biology, 1st
1217 Edition (Blackwell Pub.).

1218 23. Wooding, F.B.P., and Burton, G. (2008). Comparative placentation : structures, functions
1219 and evolution (Springer).

1220 24. Berkebile, Z.W., Putri, D.S., Abrahante, J.E., Seelig, D.M., Schleiss, M.R., and Bierle, C.J.
1221 (2021). The Placental Response to Guinea Pig Cytomegalovirus Depends Upon the
1222 Timing of Maternal Infection. Front Immunol *12*, 686415. 10.3389/fimmu.2021.686415.

1223 25. Schleiss, M.R., and McVoy, M.A. (2010). Guinea Pig Cytomegalovirus (GPCMV): A Model
1224 for the Study of the Prevention and Treatment of Maternal-Fetal Transmission. Future Virol
1225 *5*, 207-217. 10.2217/fvl.10.8.

1226 26. Gorman, M.J., Caine, E.A., Zaitsev, K., Begley, M.C., Weger-Lucarelli, J., Uccellini, M.B.,
1227 Tripathi, S., Morrison, J., Yount, B.L., Dinnon, K.H., 3rd, et al. (2018). An
1228 Immunocompetent Mouse Model of Zika Virus Infection. Cell Host Microbe *23*, 672-685
1229 e676. 10.1016/j.chom.2018.04.003.

1230 27. Fisher, S., Genbacev, O., Maidji, E., and Pereira, L. (2000). Human cytomegalovirus
1231 infection of placental cytotrophoblasts in vitro and in utero: implications for transmission
1232 and pathogenesis. J Virol *74*, 6808-6820. 10.1128/jvi.74.15.6808-6820.2000.

1233 28. Weisblum, Y., Panet, A., Zakay-Rones, Z., Vitenshtein, A., Haimov-Kochman, R.,
1234 Goldman-Wohl, D., Oiknine-Djian, E., Yamin, R., Meir, K., Amsalem, H., et al. (2015).
1235 Human cytomegalovirus induces a distinct innate immune response in the maternal-fetal
1236 interface. Virology *485*, 289-296. 10.1016/j.virol.2015.06.023.

1237 29. Schulz, J., Schilling, E., Fabian, C., Zenclussen, A.C., Stojanovska, V., and Claus, C.
1238 (2023). Dissecting Rubella Placental Infection in an In Vitro Trophoblast Model. Int J Mol
1239 Sci *24*. 10.3390/ijms24097894.

1240 30. de la Torre, E., Mulla, M.J., Yu, A.G., Lee, S.J., Kavathas, P.B., and Abrahams, V.M.
1241 (2009). Chlamydia trachomatis infection modulates trophoblast cytokine/chemokine
1242 production. J Immunol *182*, 3735-3745. 10.4049/jimmunol.0800764.

1243 31. Semmes, E.C., and Coyne, C.B. (2022). Innate immune defenses at the maternal-fetal
1244 interface. Curr Opin Immunol *74*, 60-67. 10.1016/j.coi.2021.10.007.

1245 32. Turco, M.Y., Gardner, L., Kay, R.G., Hamilton, R.S., Prater, M., Hollinshead, M.S.,
1246 McWhinnie, A., Esposito, L., Fernando, R., Skelton, H., et al. (2018). Trophoblast
1247 organoids as a model for maternal-fetal interactions during human placentation. Nature
1248 *564*, 263-267. 10.1038/s41586-018-0753-3.

1249 33. Haider, S., Meinhardt, G., Saleh, L., Kunihs, V., Gamperl, M., Kaindl, U., Ellinger, A.,
1250 Burkard, T.R., Fiala, C., Pollheimer, J., et al. (2018). Self-Renewing Trophoblast
1251 Organoids Recapitulate the Developmental Program of the Early Human Placenta. Stem
1252 Cell Reports *11*, 537-551. 10.1016/j.stemcr.2018.07.004.

1253 34. Hendrickson, P.G., Dorais, J.A., Grow, E.J., Whiddon, J.L., Lim, J.W., Wike, C.L., Weaver,
1254 B.D., Pflueger, C., Emery, B.R., Wilcox, A.L., et al. (2017). Conserved roles of mouse DUX
1255 and human DUX4 in activating cleavage-stage genes and MERVL/HERVL
1256 retrotransposons. Nat Genet *49*, 925-934. 10.1038/ng.3844.

1257 35. Bosnakovski, D., Gearhart, M.D., Toso, E.A., Ener, E.T., Choi, S.H., and Kyba, M. (2018).
1258 Low level DUX4 expression disrupts myogenesis through deregulation of myogenic gene
1259 expression. Sci Rep *8*, 16957. 10.1038/s41598-018-35150-8.

1260 36. Rickard, A.M., Petek, L.M., and Miller, D.G. (2015). Endogenous DUX4 expression in
1261 FSHD myotubes is sufficient to cause cell death and disrupts RNA splicing and cell
1262 migration pathways. Hum Mol Genet *24*, 5901-5914. 10.1093/hmg/ddv315.

1263 37. Full, F., van Gent, M., Sparrer, K.M.J., Chiang, C., Zurenski, M.A., Scherer, M.,
1264 Brockmeyer, N.H., Heinzerling, L., Sturzl, M., Korn, K., et al. (2019). Centrosomal protein
1265 TRIM43 restricts herpesvirus infection by regulating nuclear lamina integrity. Nat Microbiol
1266 *4*, 164-176. 10.1038/s41564-018-0285-5.

1267 38. Wyler, E., Franke, V., Menegatti, J., Kocks, C., Boltengagen, A., Praktiknjo, S., Walch-
1268 Ruckheim, B., Bosse, J., Rajewsky, N., Grasser, F., et al. (2019). Single-cell RNA-
1269 sequencing of herpes simplex virus 1-infected cells connects NRF2 activation to an
1270 antiviral program. Nat Commun *10*, 4878. 10.1038/s41467-019-12894-z.

1271 39. Love, M.I., Huber, W., and Anders, S. (2014). Moderated estimation of fold change and
1272 dispersion for RNA-seq data with DESeq2. Genome Biol *15*, 550. 10.1186/s13059-014-
1273 0550-8.

1274 40. Banerji, C.R.S., and Zammit, P.S. (2021). Pathomechanisms and biomarkers in
1275 facioscapulohumeral muscular dystrophy: roles of DUX4 and PAX7. EMBO Mol Med *13*,
1276 e13695. 10.15252/emmm.202013695.

1277 41. Cowley, M.V., Pruller, J., Ganassi, M., Zammit, P.S., and Banerji, C.R.S. (2023). An in
1278 silico FSHD muscle fiber for modeling DUX4 dynamics and predicting the impact of
1279 therapy. Elife *12*. 10.7554/eLife.88345.

1280 42. Arutyunyan, A., Roberts, K., Troule, K., Wong, F.C.K., Sheridan, M.A., Kats, I., Garcia-
1281 Alonso, L., Velten, B., Hoo, R., Ruiz-Morales, E.R., et al. (2023). Spatial multiomics map
1282 of trophoblast development in early pregnancy. Nature *616*, 143-151. 10.1038/s41586-
1283 023-05869-0.

1284 43. Derisoud, E., Jiang, H., Zhao, A., Chavatte-Palmer, P., and Deng, Q. (2024). Revealing
1285 the molecular landscape of human placenta: a systematic review and meta-analysis of
1286 single-cell RNA sequencing studies. Hum Reprod Update *30*, 410-441.
1287 10.1093/humupd/dmae006.

1288 44. Vento-Tormo, R., Efremova, M., Botting, R.A., Turco, M.Y., Vento-Tormo, M., Meyer, K.B.,
1289 Park, J.E., Stephenson, E., Polanski, K., Goncalves, A., et al. (2018). Single-cell
1290 reconstruction of the early maternal-fetal interface in humans. Nature *563*, 347-353.
1291 10.1038/s41586-018-0698-6.

1292 45. Jagannathan, S., Shadle, S.C., Resnick, R., Snider, L., Tawil, R.N., van der Maarel, S.M.,
1293 Bradley, R.K., and Tapscott, S.J. (2016). Model systems of DUX4 expression recapitulate
1294 the transcriptional profile of FSHD cells. Hum Mol Genet *25*, 4419-4431.
1295 10.1093/hmg/ddw271.

1296 46. Wang, D., and Shenk, T. (2005). Human cytomegalovirus UL131 open reading frame is
1297 required for epithelial cell tropism. J Virol *79*, 10330-10338. 10.1128/JVI.79.16.10330-
1298 10338.2005.

1299 47. Okae, H., Toh, H., Sato, T., Hiura, H., Takahashi, S., Shirane, K., Kabayama, Y., Suyama,
1300 M., Sasaki, H., and Arima, T. (2018). Derivation of Human Trophoblast Stem Cells. Cell
1301 Stem Cell *22*, 50-63 e56. 10.1016/j.stem.2017.11.004.

1302 48. Street, K., Risso, D., Fletcher, R.B., Das, D., Ngai, J., Yosef, N., Purdom, E., and Dudoit,
1303 S. (2018). Slingshot: cell lineage and pseudotime inference for single-cell transcriptomics.
1304 BMC Genomics *19*, 477. 10.1186/s12864-018-4772-0.

1305 49. Mariot, V., and Dumonceaux, J. (2022). Gene Editing to Tackle Facioscapulohumeral
1306 Muscular Dystrophy. Front Genome Ed *4*, 937879. 10.3389/fgeed.2022.937879.

1307 50. Winokur, S.T., Bengtsson, U., Vargas, J.C., Wasmuth, J.J., Altherr, M.R., Weiffenbach, B.,
1308 and Jacobsen, S.J. (1996). The evolutionary distribution and structural organization of the
1309 homeobox-containing repeat D4Z4 indicates a functional role for the ancestral copy in the
1310 FSHD region. Hum Mol Genet *5*, 1567-1575. 10.1093/hmg/5.10.1567.

1311 51. Himeda, C.L., Jones, T.I., and Jones, P.L. (2016). CRISPR/dCas9-mediated
1312 Transcriptional Inhibition Ameliorates the Epigenetic Dysregulation at D4Z4 and
1313 Represses DUX4-fl in FSH Muscular Dystrophy. Mol Ther *24*, 527-535.
1314 10.1038/mt.2015.200.

1315 52. Sikrova, D., Cadar, V.A., Ariyurek, Y., Laros, J.F.J., Balog, J., and van der Maarel, S.M.
1316 (2021). Adenine base editing of the DUX4 polyadenylation signal for targeted genetic
1317 therapy in facioscapulohumeral muscular dystrophy. Mol Ther Nucleic Acids *25*, 342-354.
1318 10.1016/j.omtn.2021.05.020.

1319 53. Mitsuhashi, H., Ishimaru, S., Homma, S., Yu, B., Honma, Y., Beermann, M.L., and Miller,
1320 J.B. (2018). Functional domains of the FSHD-associated DUX4 protein. Biol Open *7*.
1321 10.1242/bio.033977.

1322 54. Friedel, C.C., Whisnant, A.W., Djakovic, L., Rutkowski, A.J., Friedl, M.S., Kluge, M.,
1323 Williamson, J.C., Sai, S., Vidal, R.O., Sauer, S., et al. (2021). Dissecting Herpes Simplex
1324 Virus 1-Induced Host Shutoff at the RNA Level. J Virol *95*. 10.1128/JVI.01399-20.

1325 55. Tan, J., Franke, V., Neugebauer, E., Lagisquet, J., Kuderna, A.K., Walter, S., Ensser, A.,
1326 Landthaler, M., Stamminger, T., Gramberg, T., et al. (2024). DNA virus infections shape
1327 transposable elements activity in vitro and in vivo. Biorxiv.

1328 56. Neugebauer, E., Walter, S., Tan, J., Drayman, N., Franke, V., van Gent, M., Pennisi, S.,
1329 Veratti, P., Stein, K.S., Welker, I., et al. (2025). Herpesviruses mimic zygotic genome
1330 activation to promote viral replication. Nat Commun *16*, 710. 10.1038/s41467-025-55928-
1331 5.

1332 57. Liu, D., Matzuk, M.M., Sung, W.K., Guo, Q., Wang, P., and Wolgemuth, D.J. (1998). Cyclin
1333 A1 is required for meiosis in the male mouse. Nature Genetics *20*, 377-380. 10.1038/3855.

1334 58. Oduro, J.D., Uecker, R., Hagemeier, C., and Wiebusch, L. (2012). Inhibition of human
1335 cytomegalovirus immediate-early gene expression by cyclin A2-dependent kinase activity.
1336 J Virol *86*, 9369-9383. 10.1128/JVI.07181-11.

1337 59. Epping, M.T., Wang, L., Edel, M.J., Carlee, L., Hernandez, M., and Bernards, R. (2005).
1338 The human tumor antigen PRAME is a dominant repressor of retinoic acid receptor
1339 signaling. Cell *122*, 835-847. 10.1016/j.cell.2005.07.003.

1340 60. Kern, C.H., Yang, M., and Liu, W.S. (2021). The PRAME family of cancer testis antigens
1341 is essential for germline development and gametogenesisdagger. Biol Reprod *105*, 290-
1342 304. 10.1093/biolre/ioab074.

1343 61. Birtle, Z., Goodstadt, L., and Ponting, C. (2005). Duplication and positive selection among
1344 hominin-specific PRAME genes. BMC Genomics *6*, 120. 10.1186/1471-2164-6-120.

1345 62. Katayama, S., Ranga, V., Jouhilahti, E.M., Airenne, T.T., Johnson, M.S., Mukherjee, K.,
1346 Burglin, T.R., and Kere, J. (2018). Phylogenetic and mutational analyses of human LEUTX,
1347 a homeobox gene implicated in embryogenesis. Sci Rep *8*, 17421. 10.1038/s41598-018-
1348 35547-5.

1349 63. Lewin, T.D., Blagrove, J.R., and Holland, P.W.H. (2023). Rapid Evolution of the
1350 Embryonically Expressed Homeobox Gene LEUTX within Primates. Genome Biol Evol *15*.
1351 10.1093/gbe/evad097.

1352 64. Thaxton, J.E., Nevers, T., Lippe, E.O., Blois, S.M., Saito, S., and Sharma, S. (2013).
1353 NKG2D blockade inhibits poly(I:C)-triggered fetal loss in wild type but not in IL-10-/- mice.
1354 J Immunol *190*, 3639-3647. 10.4049/jimmunol.1203488.

1355 65. Thwaites, D.T., and Anderson, C.M. (2011). The SLC36 family of proton-coupled amino
1356 acid transporters and their potential role in drug transport. Br J Pharmacol *164*, 1802-1816.
1357 10.1111/j.1476-5381.2011.01438.x.

1358 66. Marks, J. (2019). The role of SLC34A2 in intestinal phosphate absorption and phosphate
1359 homeostasis. Pflugers Arch *471*, 165-173. 10.1007/s00424-018-2221-1.

1360 67. Yang, L., Liang, P., Yang, H., and Coyne, C.B. (2024). Trophoblast organoids with
1361 physiological polarity model placental structure and function. J Cell Sci *137*.
1362 10.1242/jcs.261528.

1363 68. Turco, M.Y., Gardner, L., Hughes, J., Cindrova-Davies, T., Gomez, M.J., Farrell, L.,
1364 Hollinshead, M., Marsh, S.G.E., Brosens, J.J., Critchley, H.O., et al. (2017). Long-term,
1365 hormone-responsive organoid cultures of human endometrium in a chemically defined
1366 medium. Nat Cell Biol *19*, 568-577. 10.1038/ncb3516.

1367 69. O'Connor, C.M., and Shenk, T. (2011). Human cytomegalovirus pUS27 G protein-coupled
1368 receptor homologue is required for efficient spread by the extracellular route but not for
1369 direct cell-to-cell spread. J Virol *85*, 3700-3707. 10.1128/JVI.02442-10.

1370 70. Cockrell, S.K., Sanchez, M.E., Erazo, A., and Homa, F.L. (2009). Role of the UL25 protein
1371 in herpes simplex virus DNA encapsidation. J Virol *83*, 47-57. 10.1128/JVI.01889-08.

1372 71. Bayer, A., Delorme-Axford, E., Sleigher, C., Frey, T.K., Trobaugh, D.W., Klimstra, W.B.,
1373 Emert-Sedlak, L.A., Smithgall, T.E., Kinchington, P.R., Vadia, S., et al. (2015). Human
1374 trophoblasts confer resistance to viruses implicated in perinatal infection. Am J Obstet
1375 Gynecol *212*, 71 e71-71 e78. 10.1016/j.ajog.2014.07.060.

1376 72. Wells, A.I., Grimes, K.A., and Coyne, C.B. (2022). Enterovirus Replication and
1377 Dissemination Are Differentially Controlled by Type I and III Interferons in the
1378 Gastrointestinal Tract. mBio *13*, e0044322. 10.1128/mbio.00443-22.

1379 73. Schmidt, U., Weigert, M., Broaddus, C., and Myers, G. (2018). Cell Detection with Star-
1380 Convex Polygons. held in Cham, 2018//. A.F. Frangi, J.A. Schnabel, C. Davatzikos, C.
1381 Alberola-López, and G. Fichtinger, eds. (Springer International Publishing), pp. 265-273.

1382 74. Johnson, W.E., Li, C., and Rabinovic, A. (2007). Adjusting batch effects in microarray
1383 expression data using empirical Bayes methods. Biostatistics *8*, 118-127.
1384 10.1093/biostatistics/kxj037.

1385 75. Hao, Y., Hao, S., Andersen-Nissen, E., Mauck, W.M., 3rd, Zheng, S., Butler, A., Lee, M.J.,
1386 Wilk, A.J., Darby, C., Zager, M., et al. (2021). Integrated analysis of multimodal single-cell
1387 data. Cell *184*, 3573-3587 e3529. 10.1016/j.cell.2021.04.048.

1388 76. Linderman, G.C., Zhao, J., Roulis, M., Bielecki, P., Flavell, R.A., Nadler, B., and Kluger,
1389 Y. (2022). Zero-preserving imputation of single-cell RNA-seq data. Nat Commun *13*, 192.
1390 10.1038/s41467-021-27729-z.

1391 77. Korsunsky, I., Millard, N., Fan, J., Slowikowski, K., Zhang, F., Wei, K., Baglaenko, Y.,
1392 Brenner, M., Loh, P.R., and Raychaudhuri, S. (2019). Fast, sensitive and accurate
1393 integration of single-cell data with Harmony. Nat Methods *16*, 1289-1296.
1394 10.1038/s41592-019-0619-0.

1395 78. Zappia, L., and Oshlack, A. (2018). Clustering trees: a visualization for evaluating
1396 clusterings at multiple resolutions. Gigascience *7*. 10.1093/gigascience/giy083.

1397 79. Dremel, S.E., and DeLuca, N.A. (2019). Genome replication affects transcription factor
1398 binding mediating the cascade of herpes simplex virus transcription. Proc Natl Acad Sci
1399 U S A *116*, 3734-3739. 10.1073/pnas.1818463116.

1400 80. Van den Berge, K., Roux de Bezieux, H., Street, K., Saelens, W., Cannoodt, R., Saeys,
1401 Y., Dudoit, S., and Clement, L. (2020). Trajectory-based differential expression analysis
1402 for single-cell sequencing data. Nat Commun *11*, 1201. 10.1038/s41467-020-14766-3.
1403